XMM

XMM-Newton SAS scientific validation - SAS V5.3.x

XMM-SOC-USR-TN-0009 Issue 1.0

C.Gabriel[1], M.Guainazzi[1], B. Altieri[1], M.Denby[2], M.Ehle[1],
M.Kirsch[1], J.Osborne[2], M.Smith[1], A.Talavera[1]

October 3, 2002

1) XMM-Newton Science Operation Center, VILSPA, ESA, Apartado 50727, E-28080 Madrid, Spain

2) XMM-Newton Science Survey Center, Department of Physics & Astronomy, University of Leicester, Leicester LE1 7RH, UK

Contents

1 Introduction

The scientific validation aims at ensuring a constant high quality of the XMM-Newton Science Analysis System (SAS). It is in principle based on the results of the analysis of a number of specific observations, both through the SAS Pipeline System (PPS) as well as interactively. It aims to establish:

- which instrumental modes are fully supported by SAS,
- which scientific products can be produced by SAS, and
- the level of accuracy associated with those products.

Details of the Scientific Validation Plan, as well as the reference dataset chosen, are given in Gabriel et al (2002). In the run corresponding to SAS V5.3 we had 10 datasets available for testing, covering completely the full range of actual possible XMM observational modes as offered to the Guest Observers.

In the following, we will list the data which had to be processed by the PPS, dataset by dataset, including the results of the default screening as applied to all XMM-Newton data after pipeline processing. The process failures will be listed with the corresponding explanations. The results of the special interactive analysis performed on some of the datasets for investigation of certain aspects of SAS analysis / calibration are presented and discussed in the following sections.

The list of calibration files used by the analysis is given in Appendix A of this document, the corresponding release notes are under http://xmm.vilspa.esa.es/ccf/releasenotes.

2 Input data

The 10 datasets tested during SV are listed in Table 2.

Instrument	Mode	Object	Data	Set nr	Comments
EPIC MOS	Full Frame	Lockmann Hole	70 0123700101	1	IA: astrometry
	”	G21.5.09	60 0122700101	2	IA: EPIC responses
	small Window	Mkn 421	165 0099280201	3	
	”	PKS2155-304	362 0124930301	10	
	Large Window	PKS0558-504	84 0125110101	4	IA: EPIC responses
	”	PKS0558-504	153 0129360201	5	IA: EPIC responses
	Timing Uncompressed	Her X-1	207 0134120101	7	IA: timing
EPIC-PN	Full Frame	Lockmann Hole	70 0123700101	1	IA: astrometry
	”	PKS0558-504	153 0129360201	5	IA: EPIC responses
	Large Window	AB Dor	185 0133120201	6	
	small Window	PKS0558-504	84 0125110101	4	IA: EPIC responses
	”	AB Dor	185 0133120201	6	
	”	Mkn 421	165 0099280201	3	
	Timing	Her X-1	207 0134120101	7	IA: timing
	”	PKS2155-304	362 0124930301	10	
	Burst	XTE J1650-500	323 0136140301	8	
	extended Full Frame	G21.5.09	60 0122700101	2	IA: EPIC responses
RGS	Spectroscopy (HCR)	PKS0558-504	84 0125110101	4	
	Spectroscopy	Mkn 421	165 0099280201	3	IA: eff. area
	”	AB Dor	185 0133120201	6	IA: wavelength scale
	”	PKS2155-304	362 0124930301	10	IA: eff. area
	”	Her X-1	207 0134120101	7	
OM	Imaging + Fast Mode	BPM 16274	261 0125320701	9	IA: astrometry

Table 1: SV test cases

3 Pipeline processing results

In this run, all the SV data could be processed to completion, except for the OM fast mode data included in the observation of BPM 16274. Due to a bug discovered in the OM fast mode chain by the scientific validation data reduction, the 5.3.0 version did not include processing of this mode. However, shortly after the release, the bug could be fixed. A posterior non-public SAS version used for the official pipeline running at SSC could process this data. The fixes are included in the public SAS version (5.3.3) from early June 2002.

3.1 Processed datasets

The PPS screening reports for each of the processed datasets, in

```
verbatim format
```

are presented here. These screening reports are produced by the SSC to highlight any anomalies in the pipeline processing, as first quality checks of every processed dataset. Therefore they should not be understood as a deep analysis of the results of each observation. To make them more comprehensive we have included some information as well as some illustrative figures. The first figures on each dataset are the observation configuration, as obtained by running the (newly introduced) SAS task *odfbrowser*, which gives an immediate picture of observation modes and filters as well as the exposure lengths, etc.

3.1.1 AB Doradus:

XMM-Newton observed AB Doradus ($\alpha_{2000} = 5^h28^m44^s.8$, $\delta_{2000} = -65°26'54'.9$) several times as routine calibration target. AB Doradus is the nearest K-type Zero-Age-Main-Sequence (ZAMS) star. The observation used in this report took place on December 12, 2000, revolution 185, lasting more than 20000 seconds.

The proposal position had a slight offset of around 5 arcsec [$\alpha_{2000} = 5^h28^m44^s.0$, $\delta_{2000} = -65°27'02'.0$] to the literature position of the source. However, the central reference telescope position was around 90" off, due to tests which were performed in this revolution. In this sense this observation constitutes a good case for testing the reliability of the analysis system with respect to wrongly placed RGS sources.

Fig. 1 shows the observation configuration as can be obtained from the SAS task *odfbrowser* in three different togglebar outputs (giving the exposure numbers and the used modes and filters respectively). Please notice that the mode names are the internal ones. The correspondence between them and the official nomenclature for the proposals is given in Appendix B.

3.1.1.1 PPS screening report

```
XMM SSC data-product screening log
Version: 26-Apr-02

Revolution  185
Obs Seq.    0133120201
Target      AB DOR
Seq_id      000694


** GENERAL COMMENTS
```

```
OM blocked
Bright source in center of EPIC images
Problems:
EPIC source detection
Some useless crosscorrelation products

EPIC comments refer, in general, to Energy-band 8.



** EPIC MOS1


FastUncompressed with Thick filter (duration  3096.6 s; 3089.2 s in image).
PrimeFullWindow with Thick filter (duration  6195.9 s; 6189.8 s in image)
The diffraction of the bright source on the RGA generates a spike (S013)
Spurious sources found in the wings of the bright source (S013)
Spurious sources found in diffraction spike


** EPIC MOS2

FastUncompressed with Thick filter (duration 3096.7 s; 3088.4 s in image)
PrimeFullWindow with Thick filter (duration 6198.5s; 6192.3 s in image).
The diffraction of the bright source on the RGA generates a spike (S014)
Spurious sources found in the wings of the bright source (S014)
Spurious sources found in diffraction spike



** EPIC PN

PrimeFullWindow with Thick filter (duration 4200.3 s; 4199.2 s in image)
PrimeLargeWindow with Thick filter (duration 4299.9 s; 4297.0 s in image).
PrimeSmallWindow with Thick filter (duration 4299.9 s; 4085.0 s in image)
Out of time events from bright source (S003)
Spurious sources detected in out of time events
Source split in two by CCD gap
Spurious sources found in the wings of the bright source (S005)


**  RGS1, RGS2


RGS1:
CCD 7 missing
Spatial map: 1 extraction regions
(bright spectrum visible)
Orders image: Bright spectrum visible within 1st and 2nd order
Spectrum plots: Bright spectra (continuum with emission lines)
```

```
RGS2:
CCD 4 missing
Comments to spectra as RGS1


** OM

Blocked. No products.


** Catalogue cross-correlation products


Some useless correlation products due to spurious sources in EPIC source list
No identifications for many XMM sources
Bright ROSAT and EPIC sources match
```

3.1.1.2 Pipeline Products results

The main products of this observation are considered satisfactory. The PPS produced EPIC image, combining the windowing MOS and PN exposures, is given in Fig.2. Clear to see are the out of time events from the PN image, but also several single faint sources in the field of view. The RGS1 spatial and order images from the PPS products are shown in Figs. 3 and 4, respectively. The source position taken by the pipeline for the selection regions derivation is the one corresponding to the computed center of the brightest source in the EPIC combined image. In this case it shows an offset to the literature value of around 3 arcsec. The PPS choice of the main EPIC source for deriving the selection regions automatically shows hereby its importance, since the regions are well centered despite the extreme large offset (87 arcsec) of the source position.

The RGS1 extracted first and second order spectra are shown in Fig.5. Notice that the wavelength energy scales plotted can be rather wrong, as in this case. The most prominent line, O VIII Ly alpha, should be at 18.969 Angstrom. A bug has been localized in the SAS task producing the plot, *rgspecplot*, while performing this validation testing. It only occurs when using the rebin option, which is default in the PPS system. The bug has been corrected already and will not be present in a future PPS version.

Results of interactive analysis on these data are given in section 4.6.

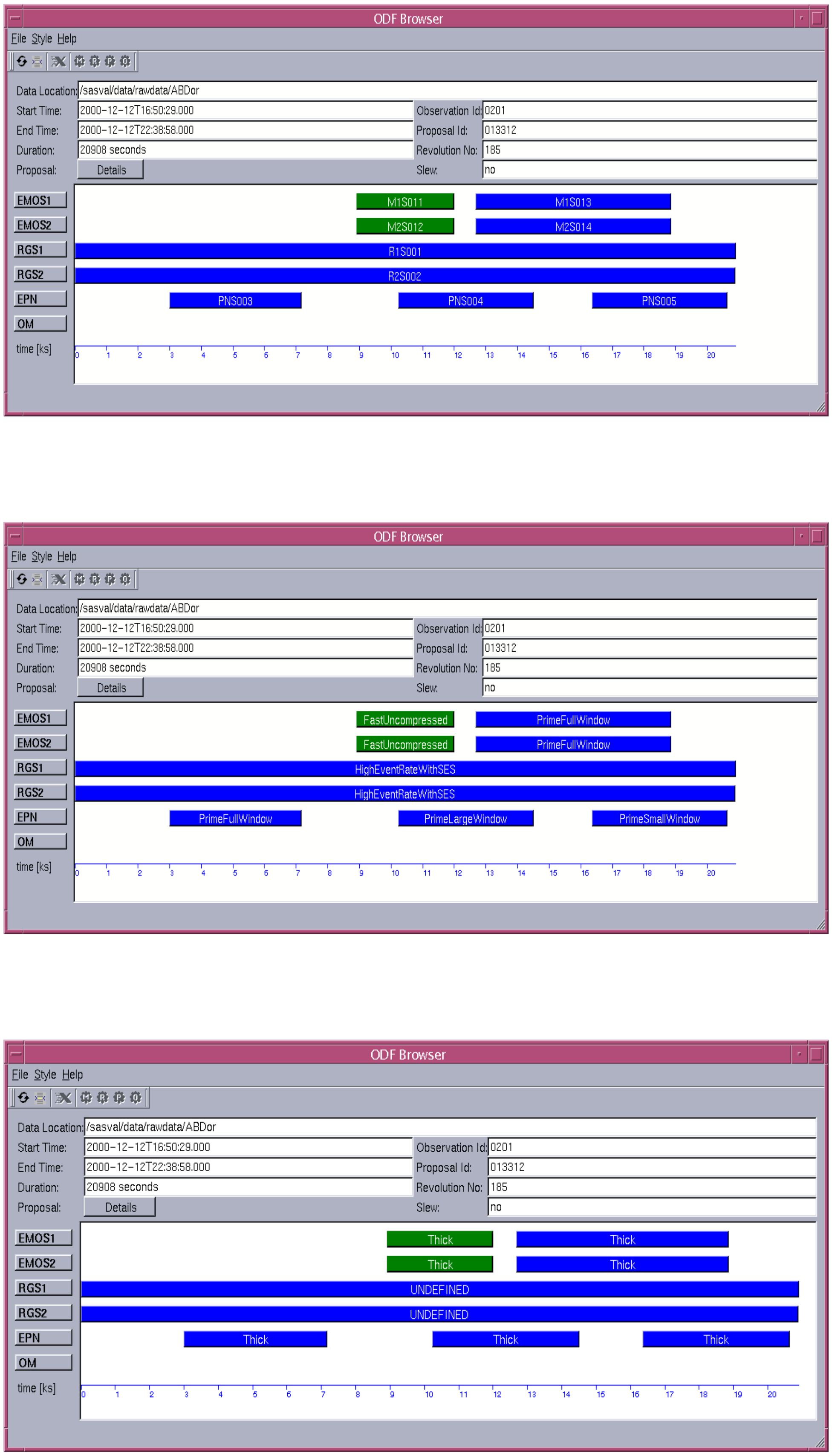

Figure 1: AB Doradus observation configuration

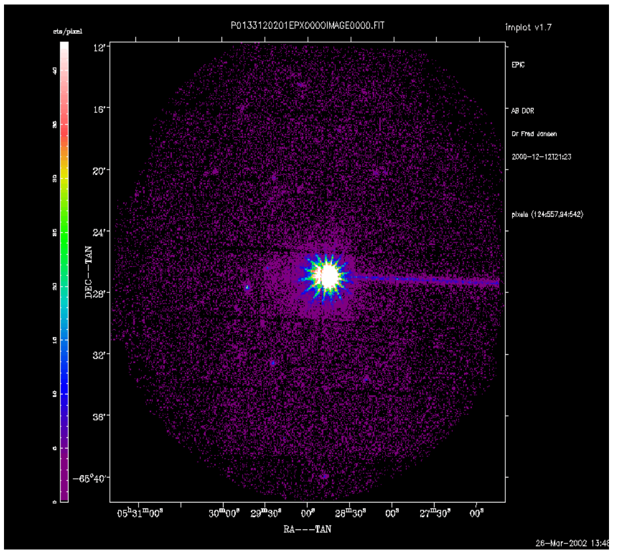

Figure 2: AB Doradus combined EPIC image

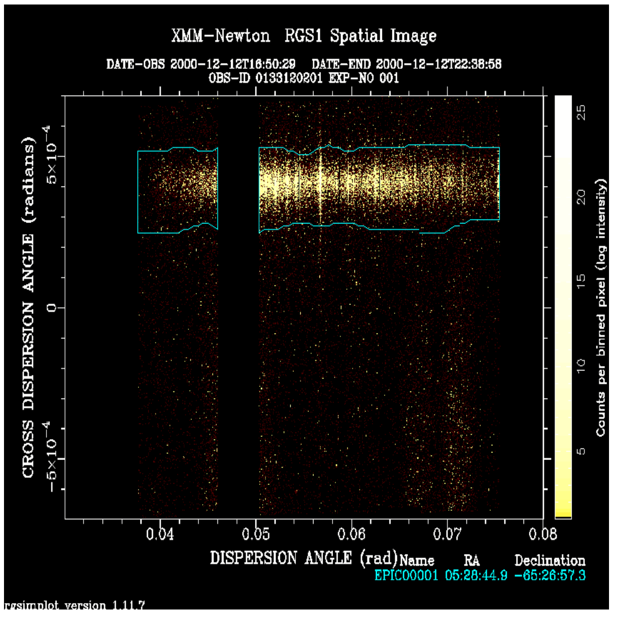

Figure 3: AB Doradus RGS1 spatial image

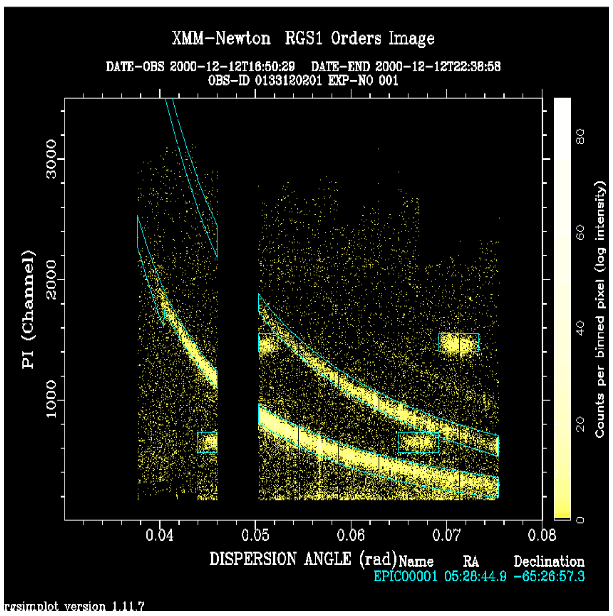

Figure 4: AB Doradus RGS1 order image

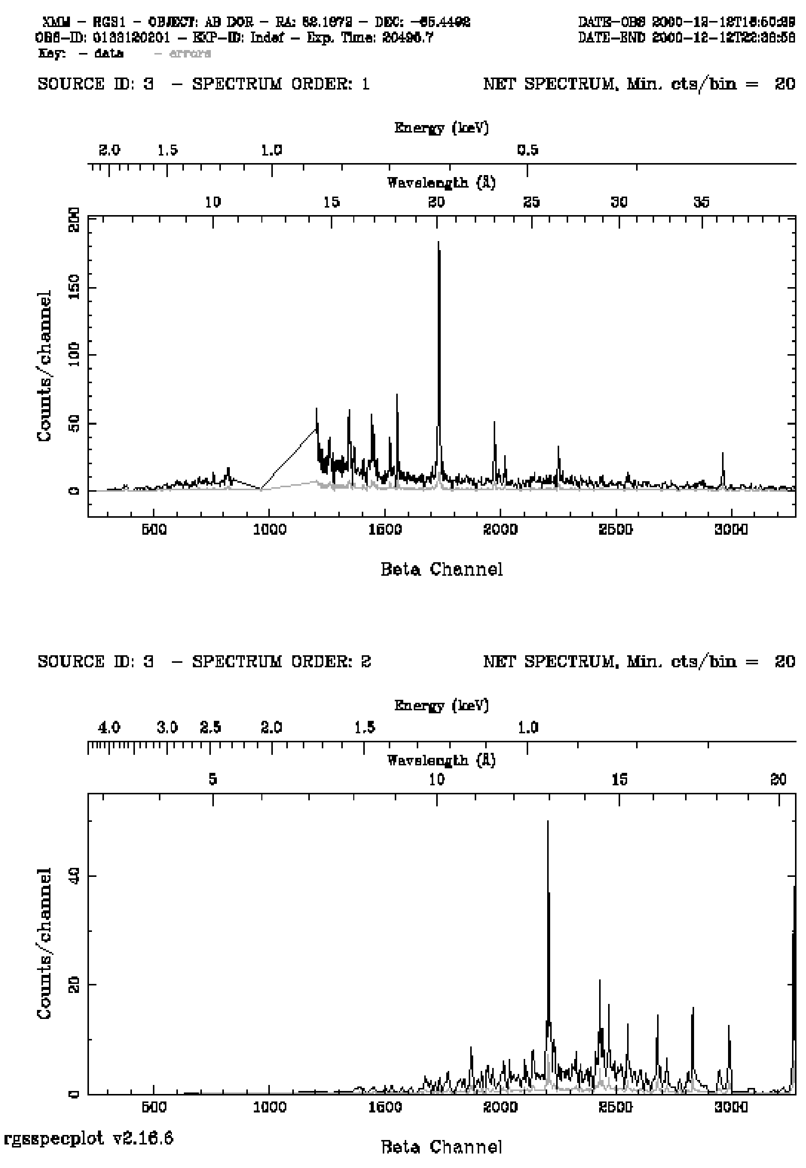

Figure 5: AB Doradus RGS1 first and second order spectra, produced by PPS. The energy and wavelength scales are wrongly placed due to a bug present in versions of rgsspecplot up to v2.16.11 (SAS V5.3.3)

3.1.2 BPM 16274

The White Dwarf BPM 16274 ($\alpha_{2000} = 0^h 50^m 3^s.18$, $\delta_{2000} = -52°08'17'.40$) is an OM calibration target. The observation used for SV was taken during revolution 261, containing 27 OM imaging exposures in 6 filters and a set of V grism exposures.

Fig. 6 shows the observation configuration (obtained using *odfbrowser*).

3.1.2.1 PPS screening report

Not available. It has not been produced at the time of writing this report.

3.1.2.2 Pipeline Products results

The processed data referred to here correspond to SAS V5.3.3, as explained under 3.

Fig. 7 shows the OM PPS final images from the observations using the V and the UVW1 filters respectively. They are both composites of five partial images taken in the standard Imaging mode. Clearly seen are the straylight features (eg. the ringlike structure right from the main source) caused by reflection of bright stars' light, like in this case, less noticeable in the UV filters. Although the features should neither affect severely source detection nor magnitude determination they make necessary in some cases parameters adjustment in the source searching procedure "omdetect" (adopting different values as the standard ones for boxscale, smoothsize, nsigma and contrast - For details see the SAS task documentation). The Xray image as obtained with the PN camera is shown in Fig. 8.

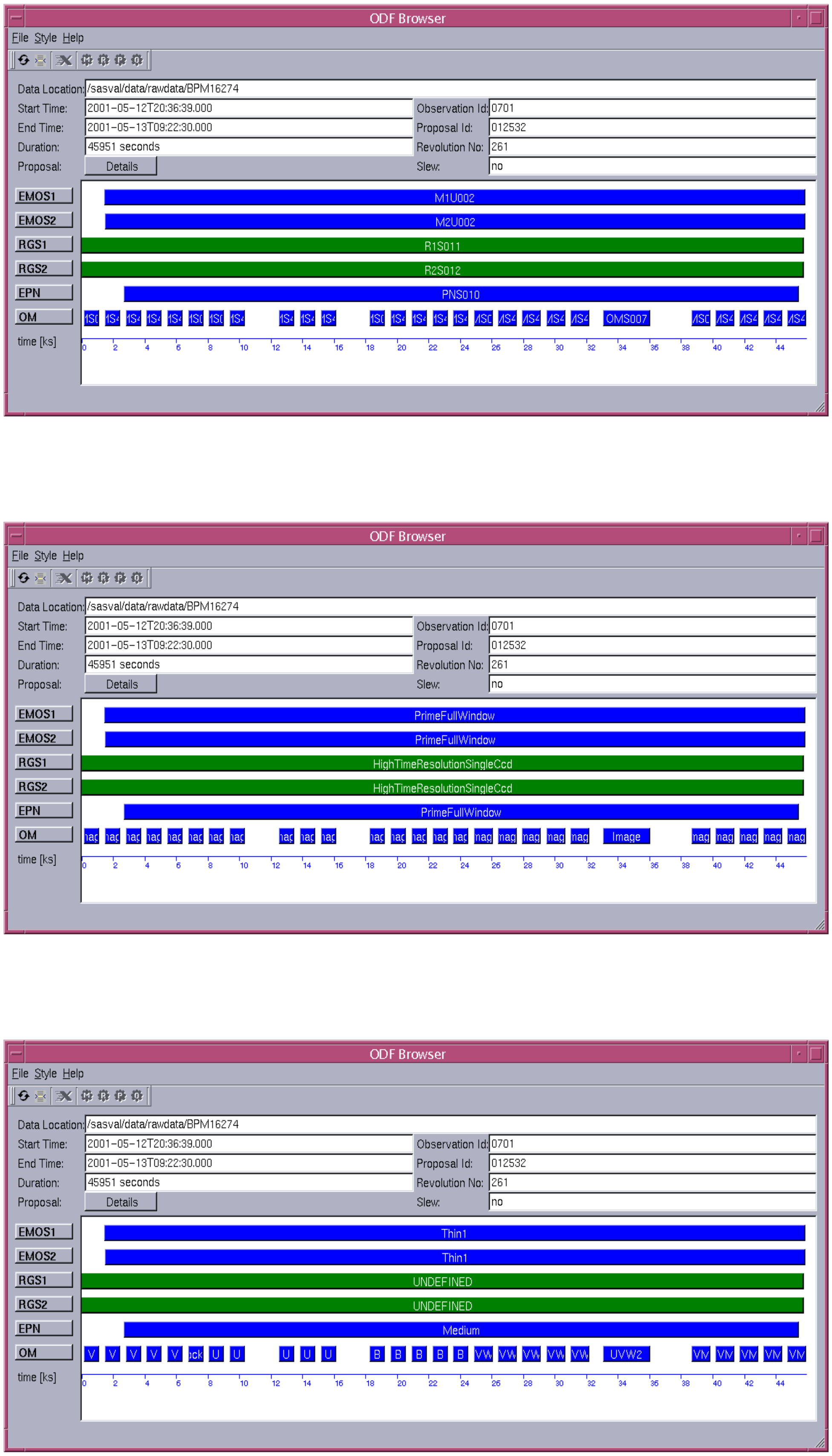

Figure 6: BPM 16274 observation configuration

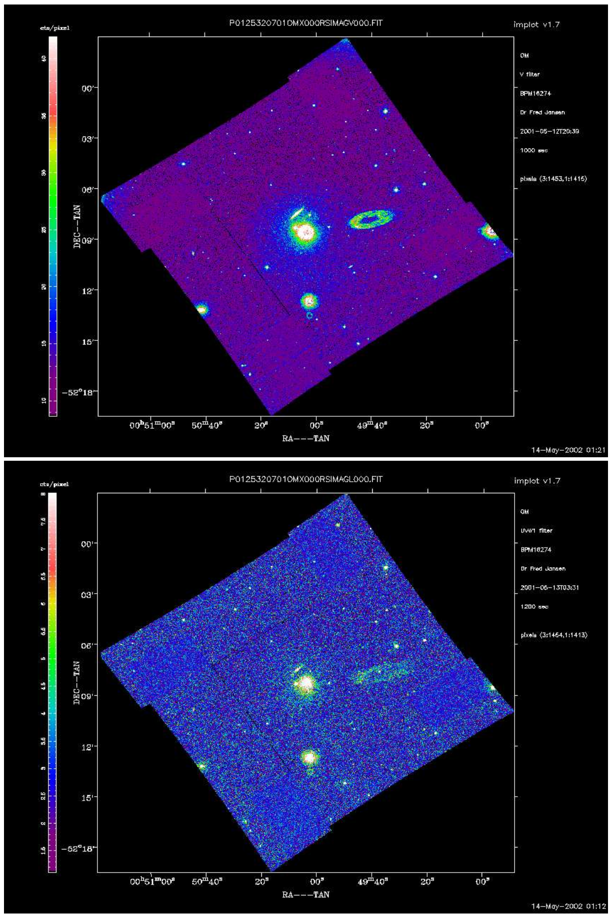

Figure 7: BPM 16274 as seen by the OM camera through the V and the UVW1 filters respectively

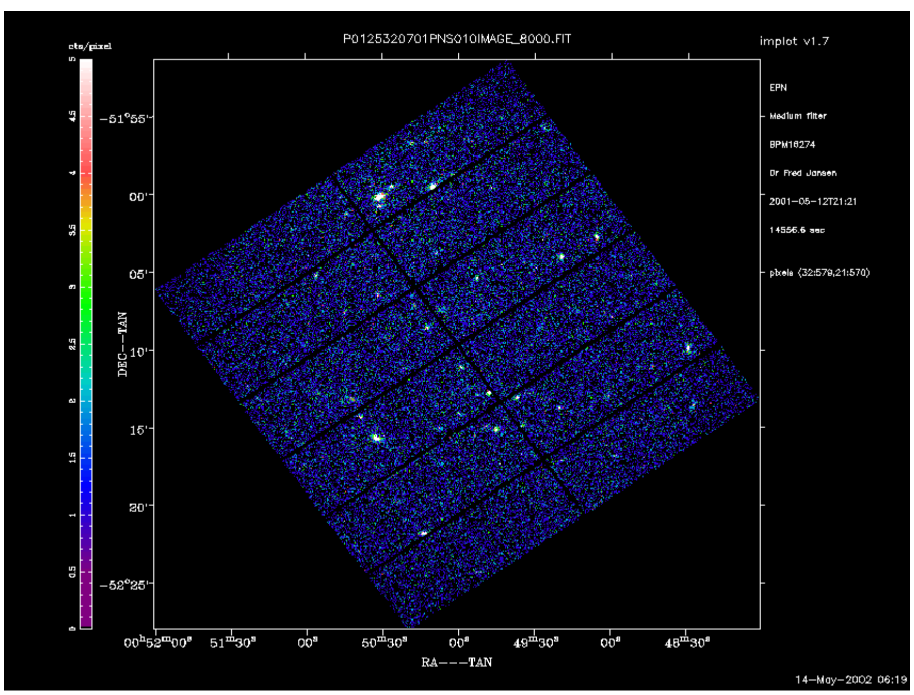

Figure 8: EPIC PN image of the BPM 16274 sky region

3.1.3 G21.5-09

XMM-Newton observed the region containing the Crab-like SuperNova Remnant (SNR) G21.5-09 ($\alpha_{2000} = 18^h33^m33^s.0$, $\delta_{2000} = -10°4534'10".0$) on April 7, 2000, between 12:35:28 and 22:57:20 UTC (revolution number 60). Warwick et al. (2001) have published preliminary scientific results of this observation.

Fig. 9 shows the observation configuration (obtained using *odfbrowser*).

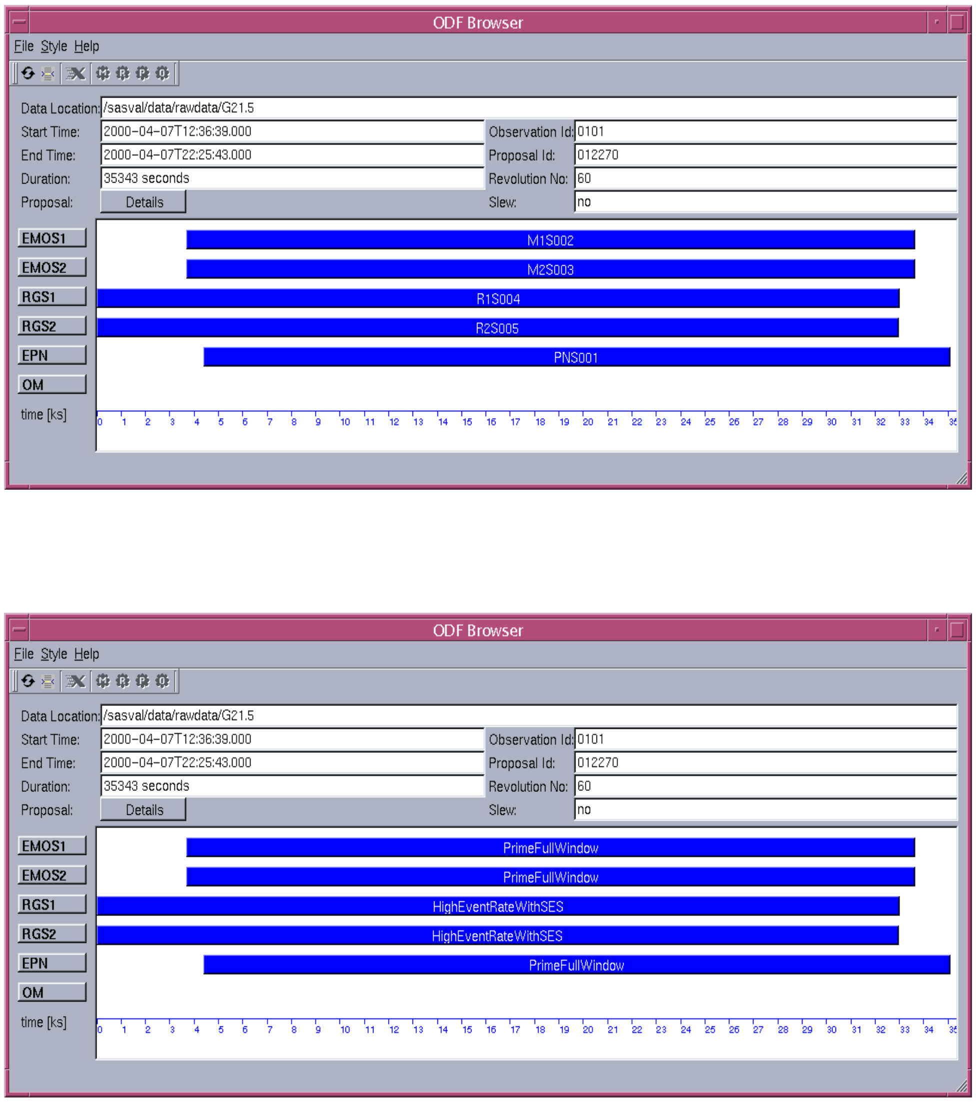

Figure 9: G21.5-09 observation configuration

3.1.3.1 PPS screening report

```
XMM SSC data-product screening log
Version: 26-Apr-02

Revolution  60
```

```
Obs Seq.    0122700101
Target      G21.5-09
Seq_id      000690


** GENERAL COMMENTS


Last observation in revolution
OM not active
Bright source in center of EPIC images
Problems:
EPIC source detection

EPIC comments refer, in general, to Energy-band 8.



** EPIC MOS1


PrimeFullWindow with Medium filter (duration 29996.6 s;  21774.0 s in image).
Spurious sources associated with extended emission


** EPIC MOS2


PrimeFullWindow with Medium filter (duration  29996.6 s; 22100.0 s in image).
Spurious sources associated with extended emission


** EPIC PN


PrimeFullWindowExtended with Medium filter (duration  30500.6 s; 19792.6 s in image).
Out of time events from bright source
Spurious sources detected in out of time events


**  RGS1, RGS2


RGS1:
CCD 7 missing
Spatial map: 1 extraction regions
(faint spectrum visible)
Orders image: Faint spectrum visible within 1st order
Spectrum plots: Noisy spectra
RGS2:
CCD 4 missing
Comments to spectra as RGS1
```

```
** OM

Not active. No products

** Catalogue cross-correlation products

Bright EPIC source not present in catalogs
Bright ROSAT and EPIC sources match
```

3.1.3.2 Pipeline Products results

X-ray images obtained with the MOS1, MOS2 (in Full Frame Mode) and PN EPIC (extended Full Frame) cameras respectively are shown in Figs. 10. Verification of the spectral fitting accuracy and of the cross-calibration among the EPIC cameras is discussed in section 4.2.1. The PPS products are considered completely acceptable, despite the spurious sources found (present in the sources lists derived), which are associated with extended emission in the EPIC MOS images and with out of time events, clearly seen in the PN image as a bright stripe above the bright extended source.

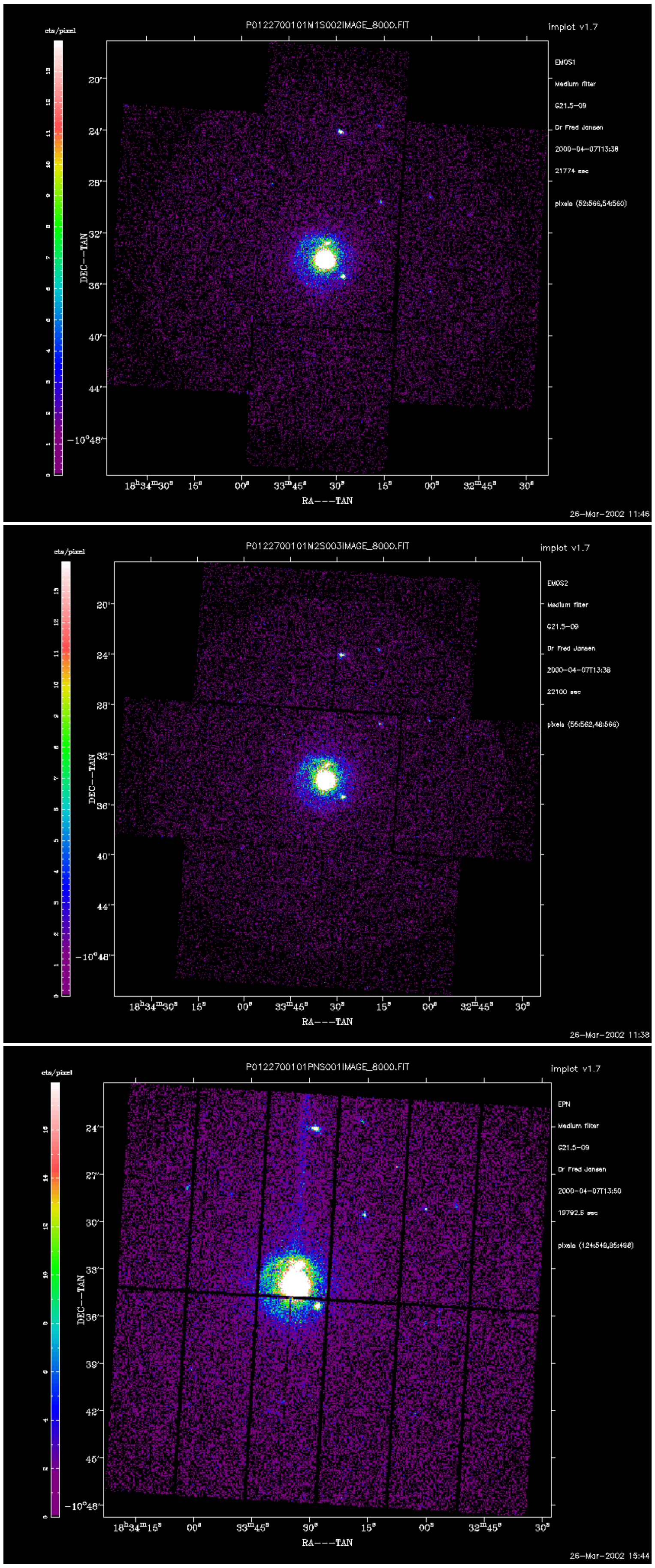

Figure 10: EPIC MOS1, MOS2 and PN images of G21.5-09

3.1.4 HER-X1

XMM-Newton observed the neutron star Hercules-X1 ($\alpha_{2000} = 16^h57^m49^s.80$, $\delta_{2000} = +35°20'32'.6$), several times. The observation used in this report took place on January 26, 2001, revolution 207, lasting for more than 9000 seconds.

Fig. 11 shows the observation configuration (obtained using *odfbrowser*).

Figure 11: Her-X1 observation configuration

3.1.4.1 PPS screening report

```
XMM SSC data-product screening log
Version: 26-Apr-02

Revolution  207
Obs Seq.    0134120101
```

```
Target      Her X-1
Seq_id      000695


** GENERAL COMMENTS

Last observation in revolution
Bright source in center of EPIC images
Problems:
EPIC source detection
OM source detection
OM tracking history plots
Many useless crosscorrelation products

EPIC comments refer, in general, to Energy-band 8.



** EPIC MOS1


FastUncompressed with Medium filter (duration  9797.0 s; 8386.4 s in image).
High background not screened in images
The diffraction of the bright source on the RGA generates a spike
Spurious sources found in diffraction spike


** EPIC MOS2


PrimeFullWindow with Medium filter (duration  10397.6 s; 9818.4 s in image).
The diffraction of the bright source on the RGA generates a spike
Spurious sources found in the wings of the bright source
Spurious sources found in diffraction spike


** EPIC PN

FastTiming with Medium filter.


**  RGS1, RGS2


RGS1:
CCD 7 missing
Spatial map: extraction region in center
Spatial map: 1 extraction regions
(bright spectrum visible)
Orders image: Bright spectrum visible within 1st and 2nd order
Spectrum plots: Bright spectra (mostly continuum)
RGS2:
```

```
CCD 4 missing
Comments to spectra as RGS1


** OM


Tracking history plots missing for exposures S011,S404,S405,S406,S407 (UVW2 filter)
2 sets of 5 exposures (Filters UVW1,UVW2;  820 s duration each)
Scattered light central enhancement
Centre of detection box shifted from centre of source


** Catalogue cross-correlation products


Catalogue positions offset from the XMM source positions
Problems with cut values in EPIC image
Bright ROSAT and EPIC sources match
Many useless correlation products due to spurious sources in EPIC source list
```

3.1.4.2 Pipeline Products results

EPIC MOS1 and EPIC PN were configured in Timing mode, the corresponding analysis is to be found under 4.3. The full combined EPIC image contains therefore in the center of the image, where the source is located, only the contribution from the MOS 2 camera, taken in Full Frame mode (Fig. 12).The very bright source is clearly piled-up to the level of showing a "hole" in the center.

The RGS spatial and energy selection regions are in this case taken from the source position as given in the proposal, matching quite well the signals as seen in Fig. 13. The complex continuum spectrum is shown in Fig. 14.

An example for the OM simultaneously taken images in two UV bands is given in Fig. 15.

All main products of this observation are considered satisfactory.

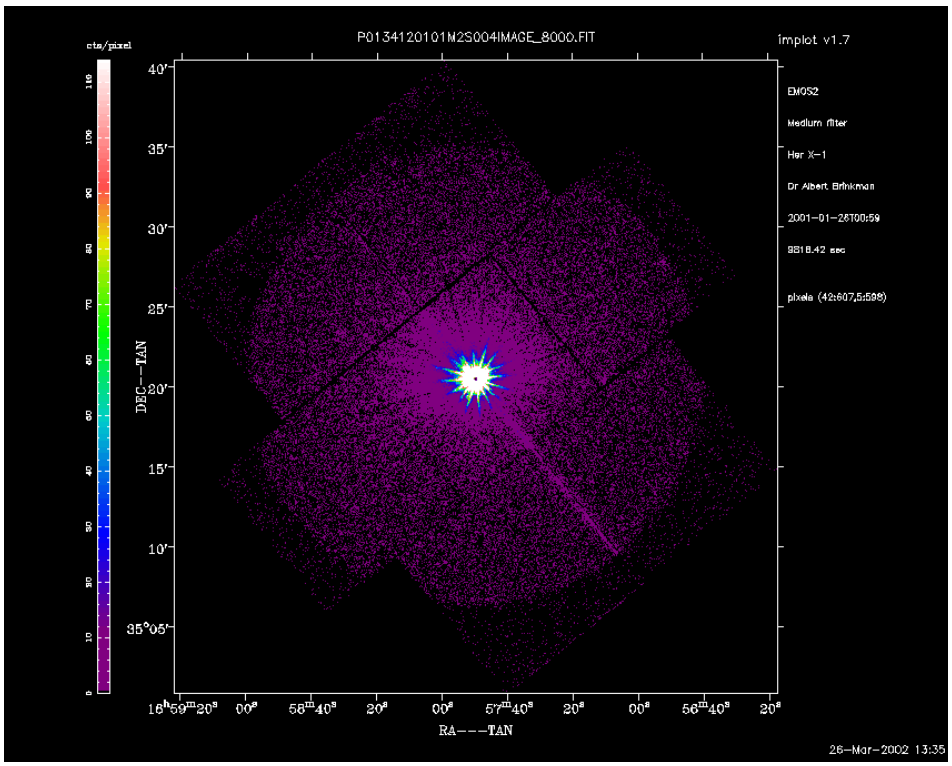

Figure 12: Her-X1 all EPIC image

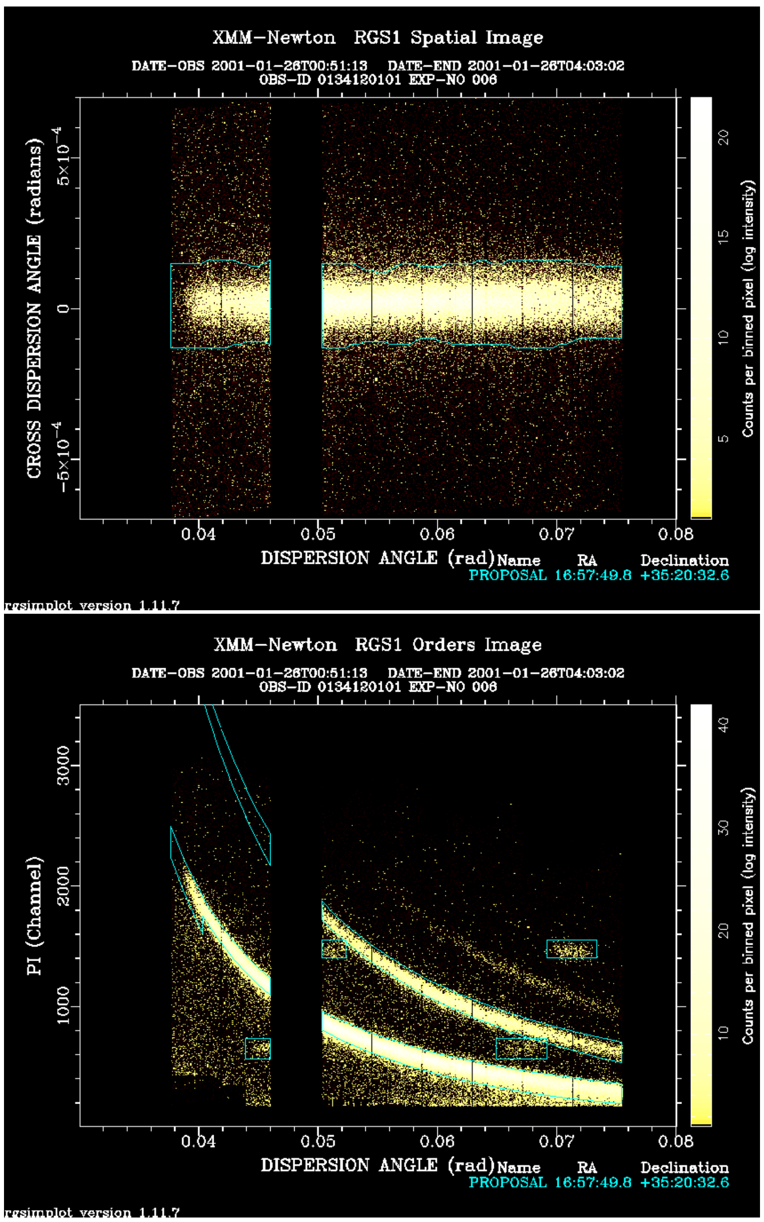

Figure 13: Her-X1 RGS1 spatial and energy plots with the corresponding selection regions

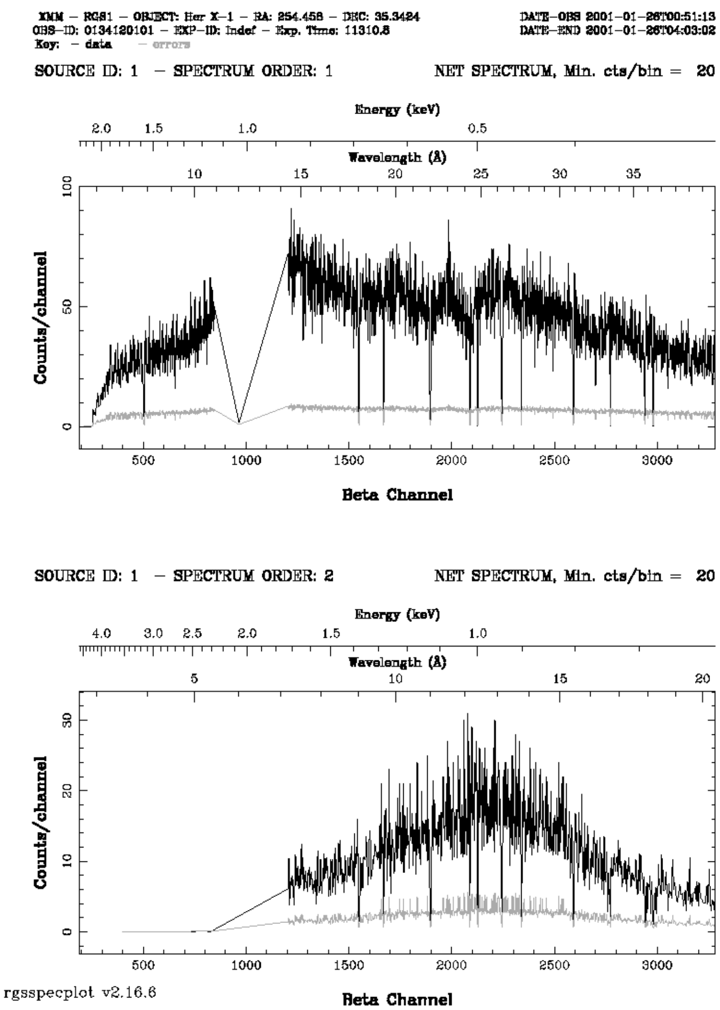

Figure 14: Her-X1 RGS1 background subtracted spectrum

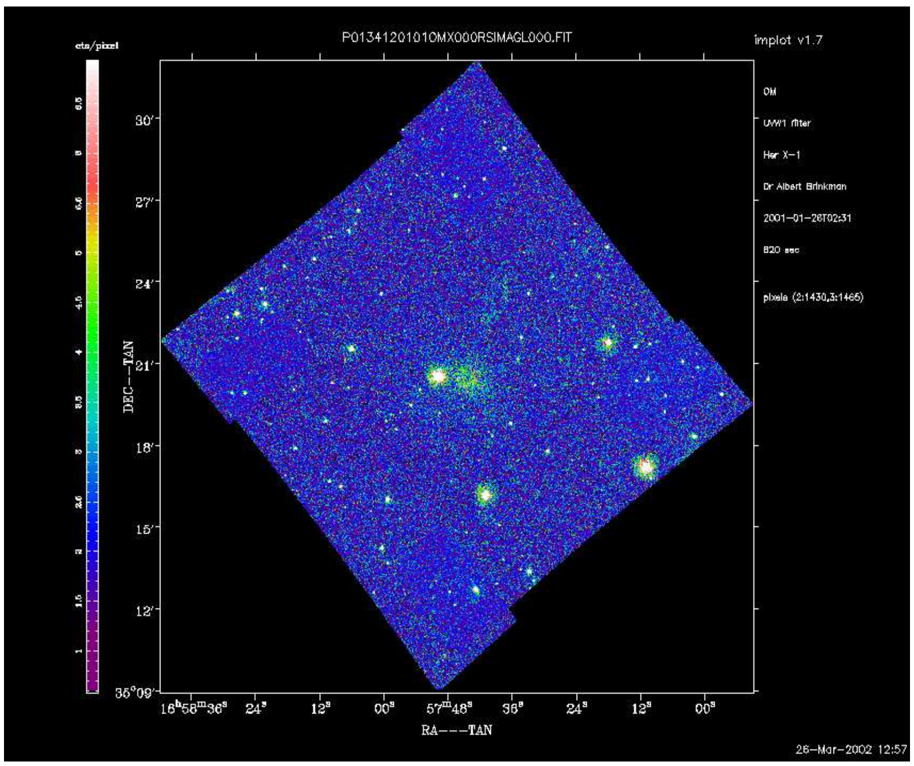

Figure 15: OM image taken with the UVW1 filter in the Her-X1 region

3.1.5 Lockman Hole

The Lockman Hole field, centered on the sky position ($\alpha_{2000} = 10^h52^m43^s.0$, $\delta_{2000} = 57°28'48".0$), one of the most observed sky areas at all wavelengths, has been observed by XMM-Newton several times. We use for scientific validation purposes the almost 70 ksec observation performed in revolution 70, on April 27, 2000, between 02.46:15 UTC and 21:37:20 UTC.

Fig. 16 shows the observation configuration (obtained using *odfbrowser*).

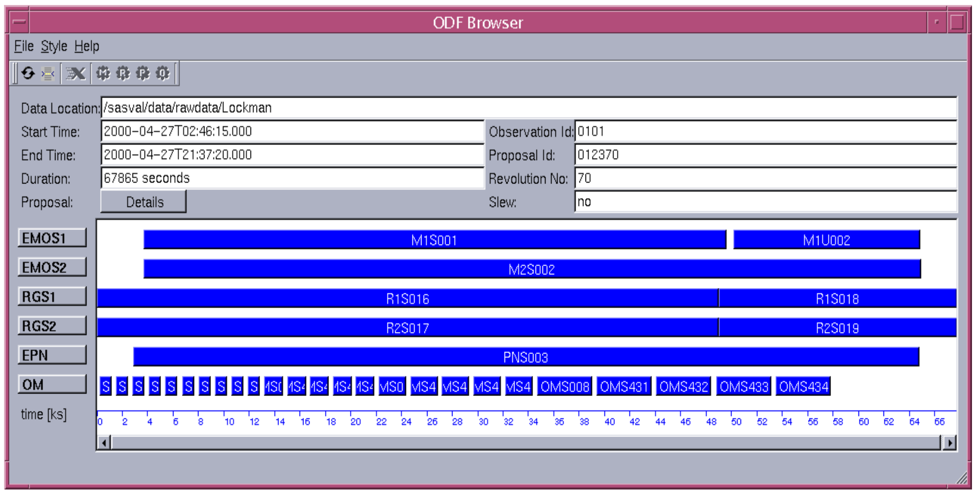

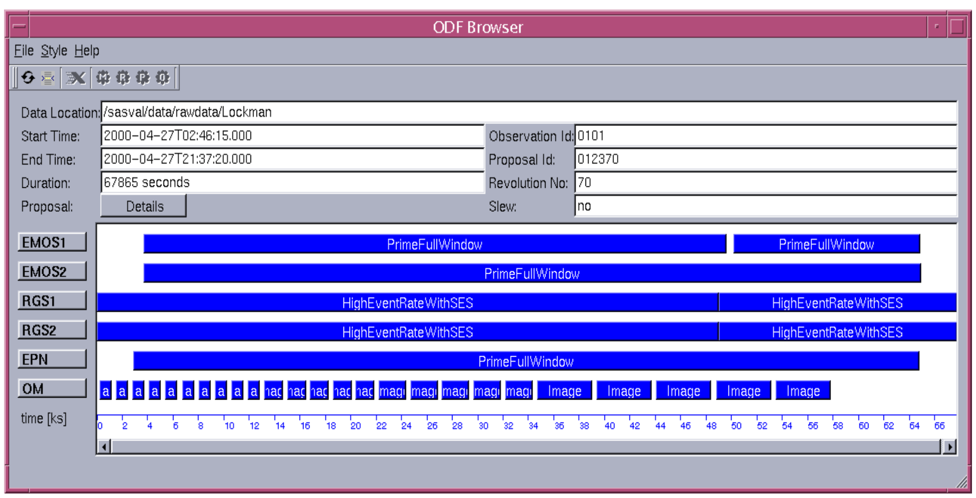

Figure 16: Lockman Hole observation configuration

3.1.5.1 PPS screening report

```
XMM SSC data-product screening log
Version: 26-Apr-02
```

```
Revolution  70
Obs Seq.    0123700101
Target      Lockman Hole
Seq_id      000689


** GENERAL COMMENTS

First observation in revolution
No bright source in center of EPIC images

Problems:
OM tracking history plots

EPIC comments refer, in general, to Energy-band 8.



** EPIC MOS1


PrimeFullWindow with Thin1 filter (duration 45859.4 s; 34268.0 s in image).
PrimeFullWindow with Thin1 filter (duration 14773.0 s; 41.6 s in image).

** EPIC MOS2


PrimeFullWindow with Thick filter (duration 61295.7s; 37076.0 s in image).


** EPIC PN


PrimeFullWindow with Thin1 filter (duration  61800.5 s; 34680.0 s in image).
Two sources detected as one.


**  RGS1, RGS2

RGS1: S016
Spatial map: 1 extraction regions
(no spectrum visible)
Orders image: No spectrum visible within 1st and 2nd order
Spectrum plots: Noisy spectra

RGS1: S018
Spatial map: 1 extraction regions
(no spectrum visible)
Orders image: No spectrum visible within 1st and 2nd order
Spectrum plots: Noisy spectra with lines

RGS2: S017
```

```
CCD 4 missing
Comments to spectra as RGS1 S016

RGS2: S019
CCD 4 missing
Comments to spectra as RGS1 S018



** OM

Tracking history plots missing for images with UVW2 filter.
Scattered light features
Ghost rings
Dark spots (reduced response - ‘holes’)



** Catalogue cross-correlation products

Bright EPIC source not present in catalogs
Catalogue positions offset from the XMM source positions
Bright ROSAT and EPIC sources match
```

3.1.5.2 Pipeline Products results

All main products of this observation are considered satisfactory. The extreme sensitivity of XMM-Newton is clearly seen in the EPIC composite image of this observation, Fig. 17. The corresponding astrometric results are given in section 4.1.

The observation with the OM include all filters. Fig. 18 shows the image in the V-filter. The straylight artifacts caused by the brightest sources in the field are clearly seen in the center of the image. The rest of the image shows a very low background and a high quality.

3.1.6 Markarian 421

The BL Lac object Markarian 421, ($\alpha_{2000} = 11^h04^m27^s.0$, $\delta_{2000} = 38°12'32".0$), is one of the RGS calibration targets. The observation used for this observation was performed in the orbit 165 with an observation length of approximately 40 ksec.

A single exposure in small window mode was chosen for all 3 EPIC cameras, as shown in the observation configuration figure (Fig. 19).

3.1.6.1 PPS screening report

```
XMM SSC data-product screening log
Version: 26-Apr-02

Revolution  165
Obs Seq.    0099280201
Target      Mkn 421
```

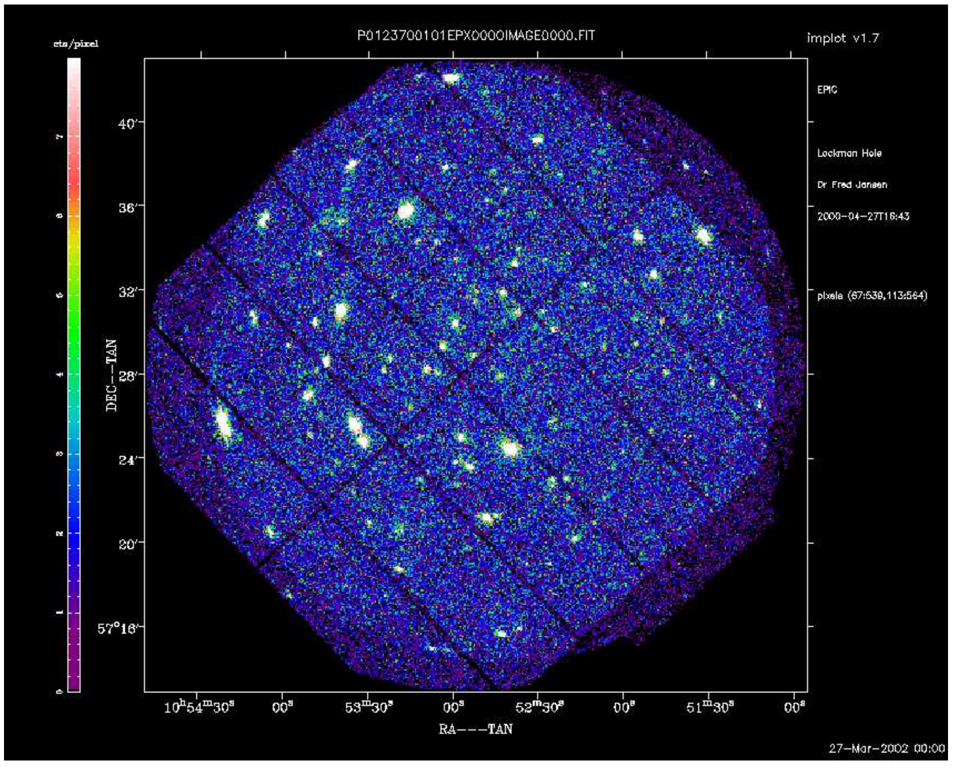

Figure 17: PPS composite EPIC image of the Lockman Hole sky area

Seq_id 000691

** GENERAL COMMENTS

OM blocked
Bright source in center of EPIC images
First observation in revolution
Problems:

EPIC source detection

EPIC comments refer, in general, to Energy-band 8.

** EPIC MOS1

PrimePartialW2 with Medium filter (duration 37251.5 s; 33402.5s in image).
High background not totally screened in images
Bright segments of rows/columns in band 8000 (usually 1)
Spurious sources found in bright segments of rows/columns
Spurious sources associated with extended emission

** EPIC MOS2

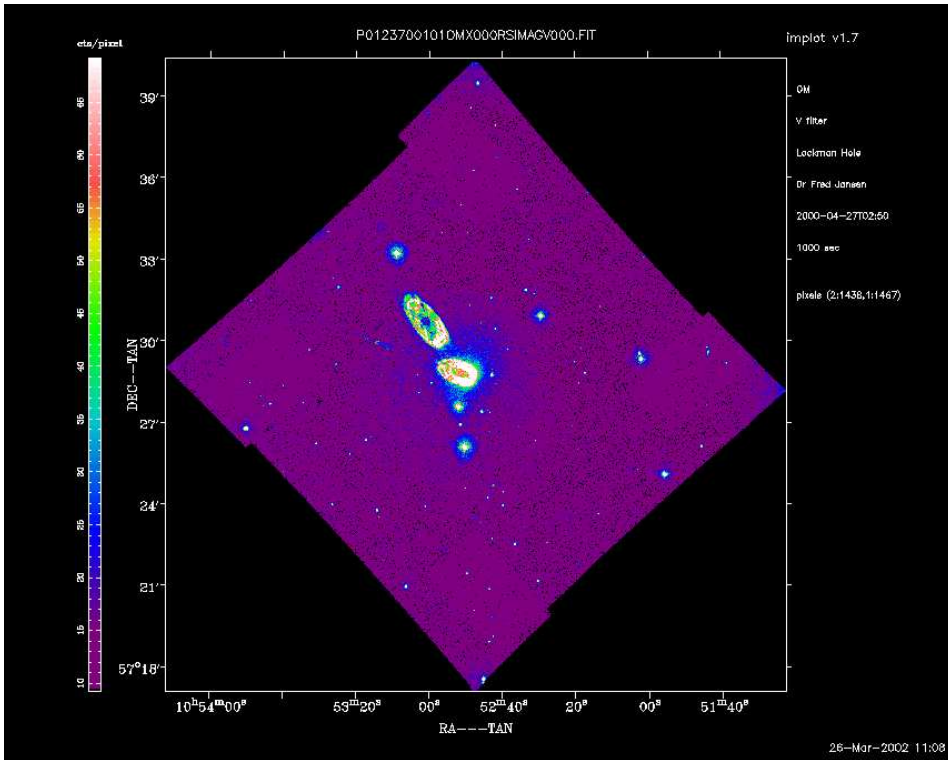

Figure 18: Optical Monitor V-filter image of the Lockman Hole

```
PrimePartialW2 with Medium filter (duration 37250.8 s; 33638.0 s in image).
High background not totally screened in images
Bright segments of rows/columns in band 8000 (usually 1)
Spurious sources found in bright segments of rows/columns
Spurious sources associated with extended emission

** EPIC PN


PrimeSmallWindow with Thick filter (duration  36900.2 s; 34541.0 s in image).


**  RGS1, RGS2


RGS1:
CCD 7 missing
Spatial map: 1 extraction regions
(bright spectrum visible)
Orders image: Bright spectrum visible within 1st and 2nd order
Spectrum plots: Bright spectra (mostly continuum)
RGS2:
CCD 4 missing
Comments to spectra as RGS1
```

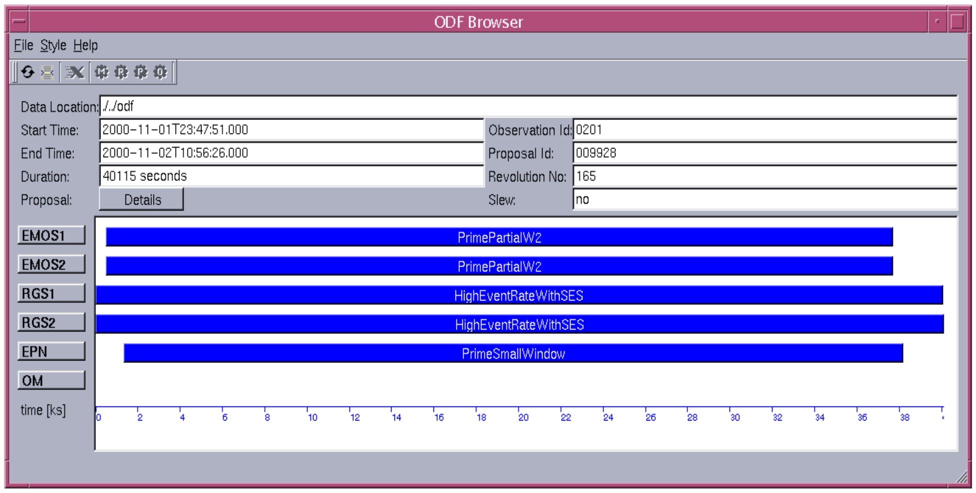

Figure 19: Markarian 421 observation configuration

```
** OM

Blocked. No products

** Catalogue cross-correlation products

Bright ROSAT and EPIC sources match
Extended ROSAT and EPIC source match
Catalogue positions offset from the XMM source positions
```

3.1.6.2 Pipeline Products results

The image products of the EPIC exposures in Small Window mode both for MOS1 and PN are shown in Fig. 20. Plots of the spatial and energy selection regions corresponding to the RGS2 are shown in Fig. 21. The corresponding first and second order background subtracted spectra are given in Fig. 22.

All the main PPS products of these observation are considered satisfactory. The results of the interactive analysis of this data are given in 4.5.

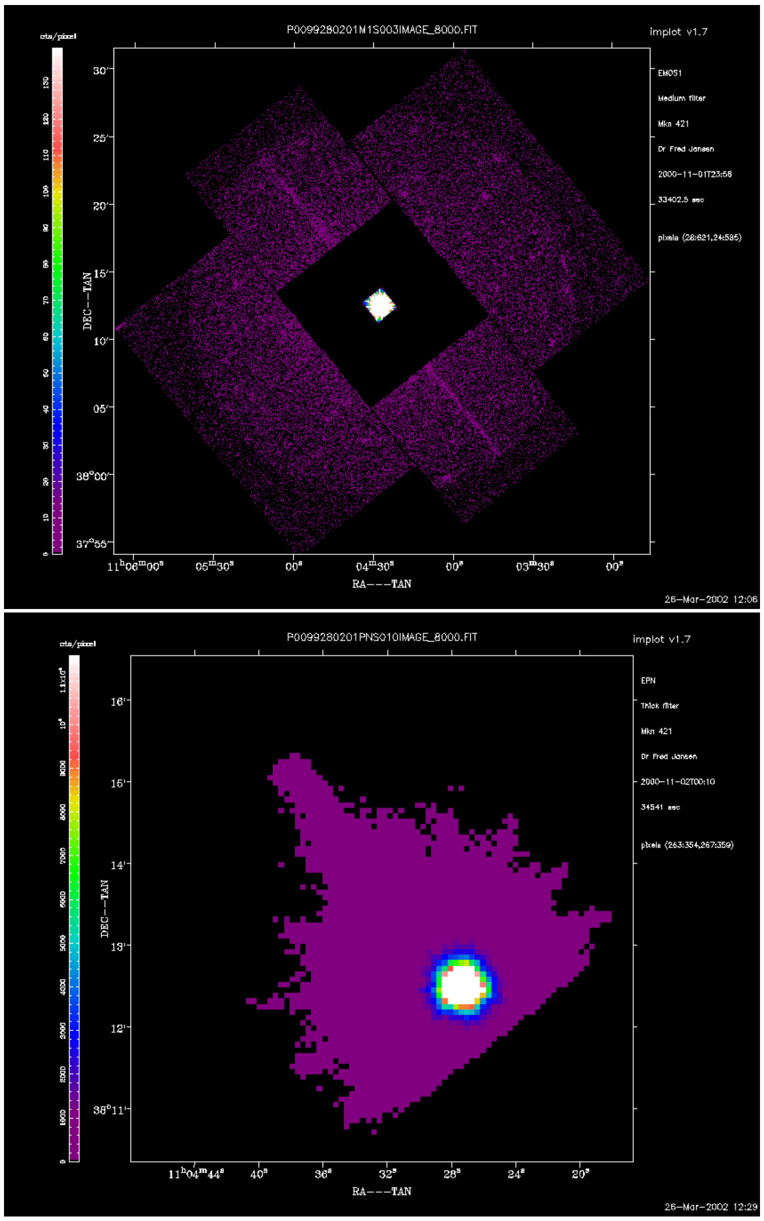

Figure 20: Mkn421 EPIC-MOS1 and -PN small window mode images

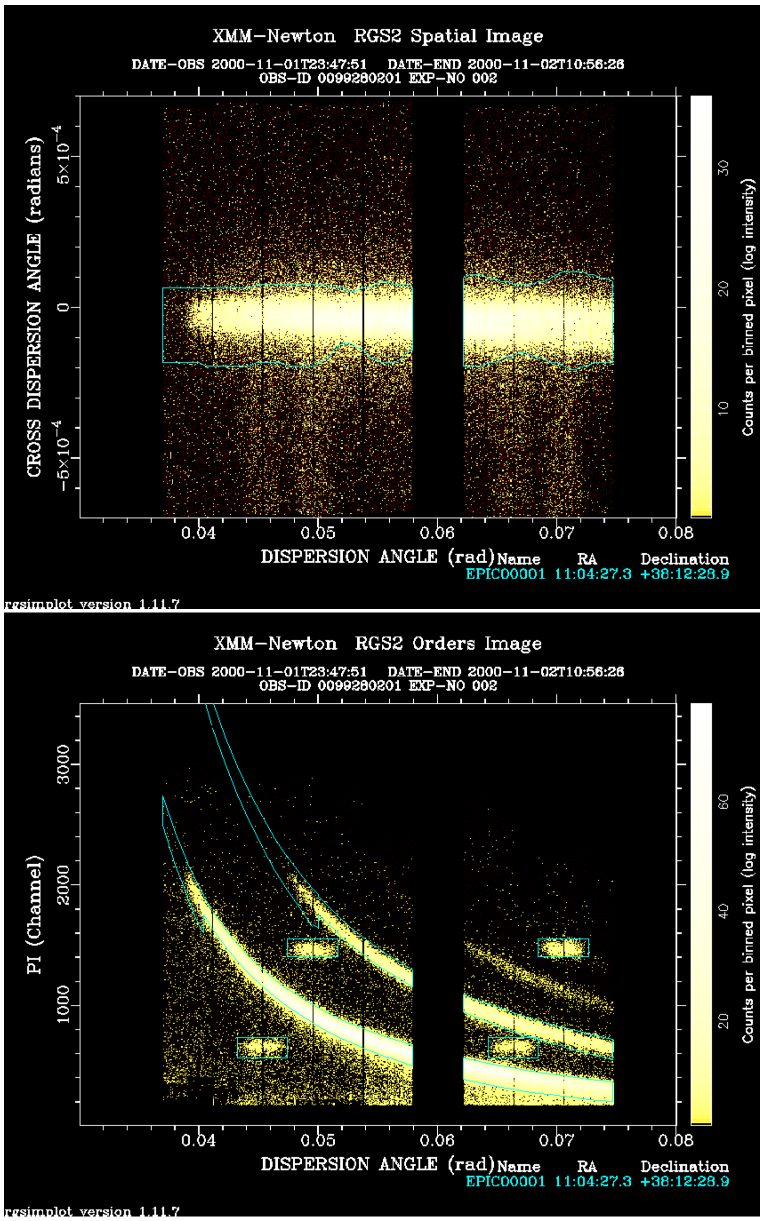

Figure 21: Mkn421 RGS2 spatial and energy plots with the corresponding selection regions

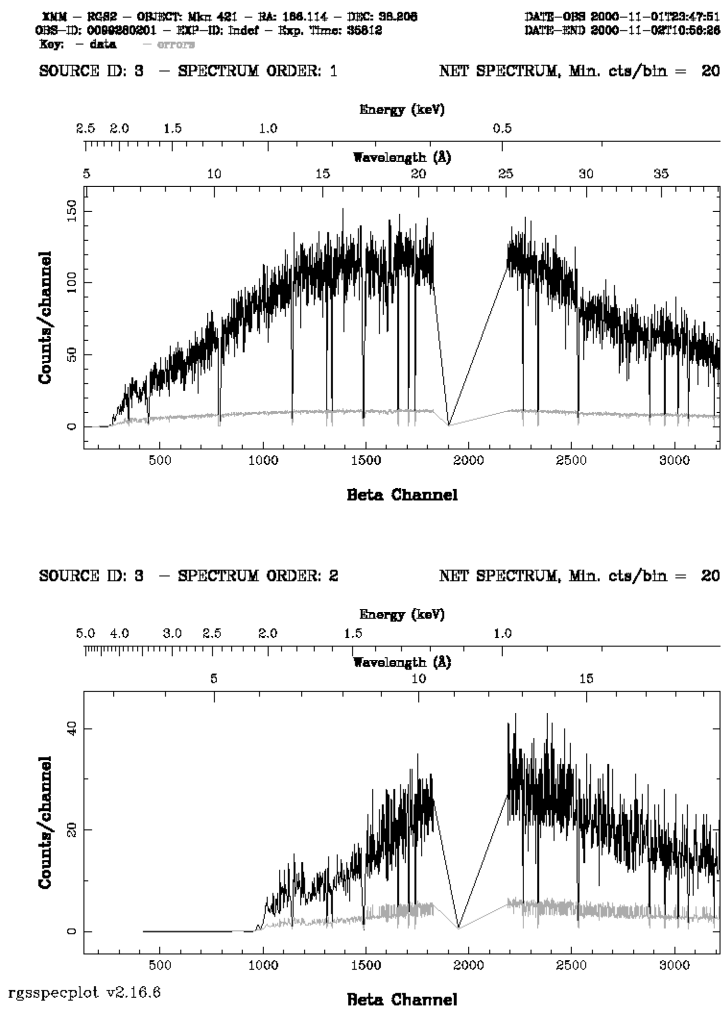

Figure 22: Mkn421 background subtracted spectrum

3.1.7 PKS 0558-504

The bright quasar PKS 0558 - 504 observation ($\alpha_{2000} = 05^h 59^m 47^s.0$, $\delta_{2000} = -50°26'51".0$) we use for validation has been performed in revolution 84 and 153. It was used for final commissioning of the OM Fast Mode.

<u>Revolution 84:</u>

The observation configuration for this observation is shown in Fig. 23.

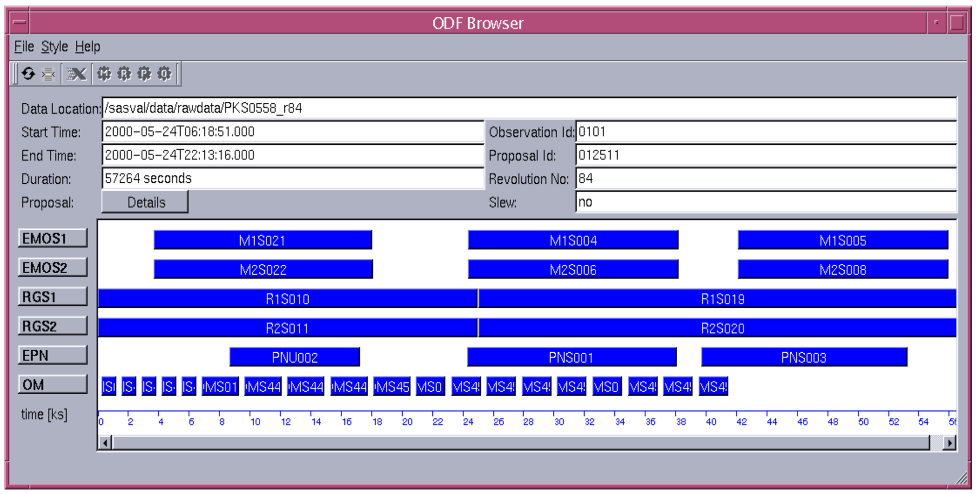

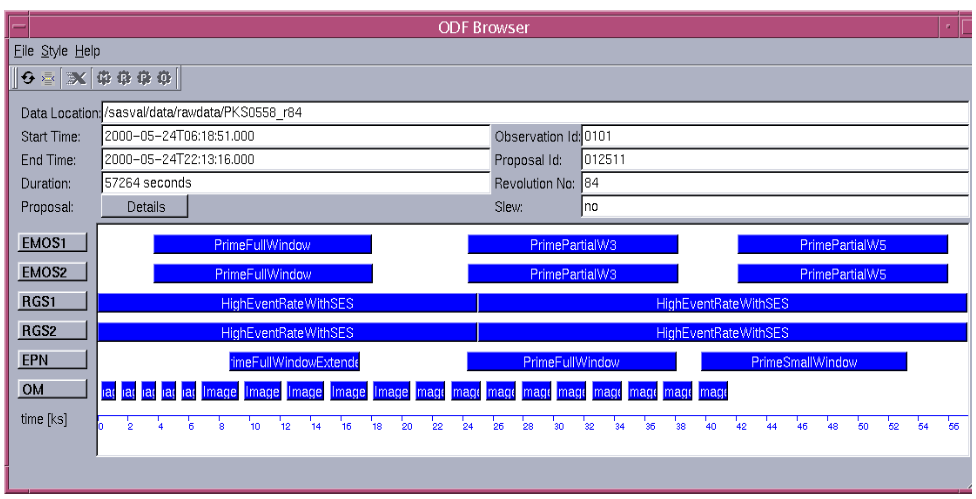

Figure 23: PKS 0558 observation configuration in rev 84

3.1.7.1 PPS screening report

```
XMM SSC data-product screening log
Version: 26-Apr-02

Revolution  84
```

```
Obs Seq.    0125110101
Target      PKS0558-504
Seq_id      000692


** GENERAL COMMENTS


First observation in revolution
OM partly with filter Grism1 or Grism2 or Magnifier
Bright source in center of EPIC images
Problems:
EPIC source detection
OM source detection
ROSAT overlay
Many useless crosscorrelation products

EPIC comments refer, in general, to Energy-band 8.



** EPIC MOS1

PrimePartialW3 with Medium filter (duration 13898.9 s; 3276.0s in image).
PrimePartialW5 with Medium filter (duration  13900.7 s; 2756.0 s in image).
Spurious sources found in the wings of the bright source
Bright pixels in bands 1,8
Spurious sources found in bright pixels
Flaring activity at end of exposure


** EPIC MOS2

PrimePartialW3 with Medium filter (duration 13899.8 s; 3432.0s in image).
PrimePartialW5 with Medium filter (duration 13900.2 s ; 2704.0 s in image).
Spurious sources found in the wings of the bright source
Flaring activity at end of exposure


** EPIC PN

PrimeFullWindow with Medium filter (duration 13599.0 s; 4510.0 s in image).
PrimeSmallWindow with Medium filter (duration 13599.7 s; 4200.0 s in image).
Out of time events from bright source
Spurious sources detected in out of time events
Spurious sources found in the wings of the bright source
Flaring activity at start of exposure
Flaring activity at end of exposure


**  RGS1, RGS2
```

```
RGS1:
Spatial map: extraction region in center
Spatial map: 1 extraction regions
(bright spectrum visible)
Orders image: Bright spectrum visible within 1st and 2nd order
Spectrum plots: Bright spectra (mostly continuum)
RGS2:
CCD 4 missing
Comments to spectra as RGS1


** OM


Tracking history plots missing for UVW2 filter exposures
Exposures from RUDI-5 set missing (filter UVW2)
Readout streaks
Ghost rings
Scattered light central enhancement
Scattered light features
Source detection problems:
Spurious sources in diffuse features
Centre of detection box shifted from centre of source



** Catalogue cross-correlation products


Bright ROSAT and EPIC sources match
Problem with cut values in ROSAT overlay
Many useless correlation products due to spurious sources in EPIC source list
```

3.1.7.2 Pipeline Products results

Fig. 24 shows the MOS1 and 2 images taken in Partial W3 (Large Window) and Partial W5 (Small Window) modes, and the PN images in Full Frame and Small Window modes. All exposures were performed with the MEDIUM filter. The EPIC data set is considered acceptable. A deeper analysis of these products follows in section 4.

Revolution 153:

The configuration of the observation in rev. 153 is shown in 25.

3.1.7.3 PPS screening report

```
XMM SSC data-product screening log
Version: 26-Apr-02

Revolution  153
```

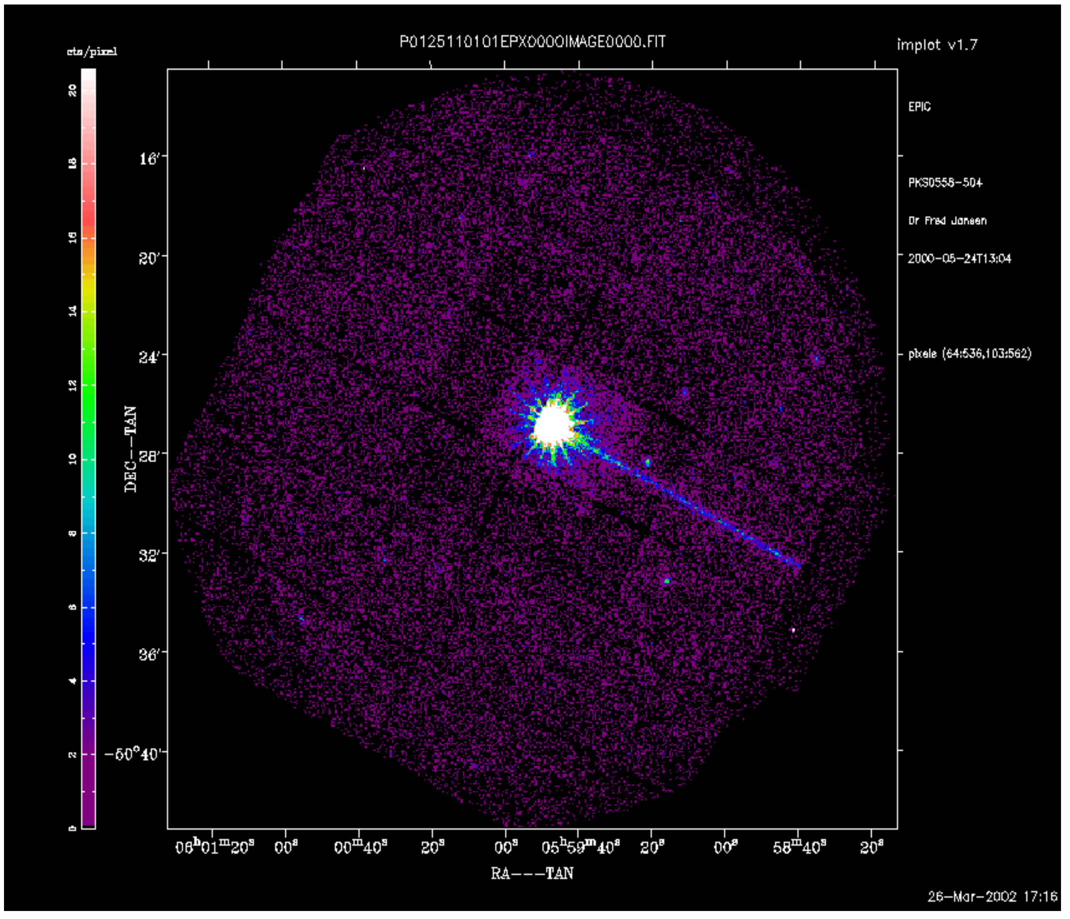

Figure 24: EPIC observation image of PKS 0558–504 in revolution 84

```
Obs Seq.    0129360201
Target      PKS0558-504 (FAST t
Seq_id      000699
```

** GENERAL COMMENTS

Last observation in revolution
OM partly with filter Grism1 or Grism2 or Magnifier
Bright source in center of EPIC images
Problems:
EPIC source detection
OM source detection
ROSAT overlay
Many useless crosscorrelation products

EPIC comments refer, in general, to Energy-band 8.

** EPIC MOS1

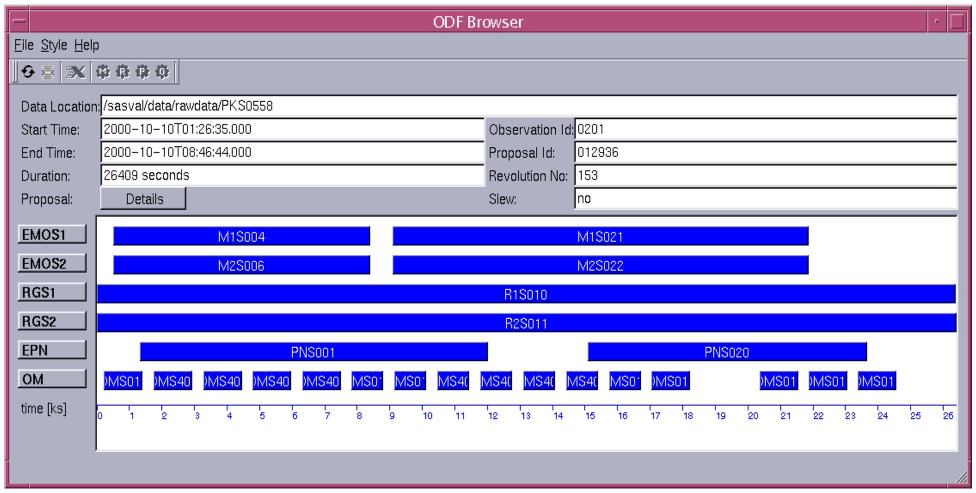

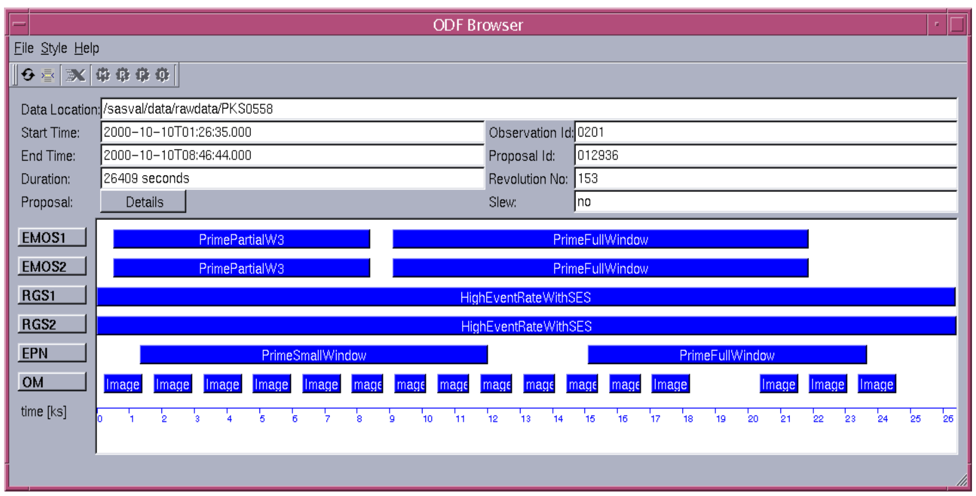

Figure 25: PKS 0558 observation configuration in rev 153

```
PrimePartialW3 with Thin1 filter (duration  7900.3 s; 7881.5 s in image).
PrimeFullWindow with Thin1 filter (duration 12797.4s; 12789.8 in image).

** EPIC MOS2

PrimePartialW3 with Thin1 filter (duration  7899.4s; 7890.3 s in image)
PrimeFullWindow with Thin1 filter (duration 12797.4 s; 12791.8 s in image).
The diffraction of the bright source on the RGA generates a spike
Spurious sources found in diffraction spike


** EPIC PN
```

```
PrimeSmallWindow with Thin1 filter (duration 10700.0 s; 10681.4 s in image).
PrimeFullWindow with Thin1 filter (duration 8600.0 s; 8593.9 s in image).
Out of time events from bright source (S020)
Spurious sources detected in out of time events (S020)
Source split in two by CCD gap (S020)


**  RGS1, RGS2


RGS1:
CCD 7 missing
Spatial map: extraction region in center
Spatial map: 1 extraction regions
(bright spectrum visible)
Orders image: Bright spectrum visible within 1st and 2nd order
Spectrum plots: Bright spectra (mostly continuum)
RGS2:
CCD 4 missing
Comments to spectra as RGS1


** OM


2 sets of 5 exposures (Filters V, UVW1   ;  1200 s duration each)
Ghost rings
Readout streaks
Spurious sources in diffuse features
Centre of detection box shifted from centre of source


** Catalogue cross-correlation products


Problem with cut values in ROSAT overlay
Bright ROSAT and EPIC sources match
No identifications for many XMM sources
Many useless correlation products due to spurious sources in EPIC source list
```

3.1.7.4 Pipeline Products results

Fig. 26 shows the MOS1 and 2 images taken in Full Window and Partial W3 (Large Window) modes, and the PN images in Full Frame and Small Window modes. All exposures were performed with the THIN filter. The EPIC data set is considered acceptable. A deeper analysis of these products follows in section 4.

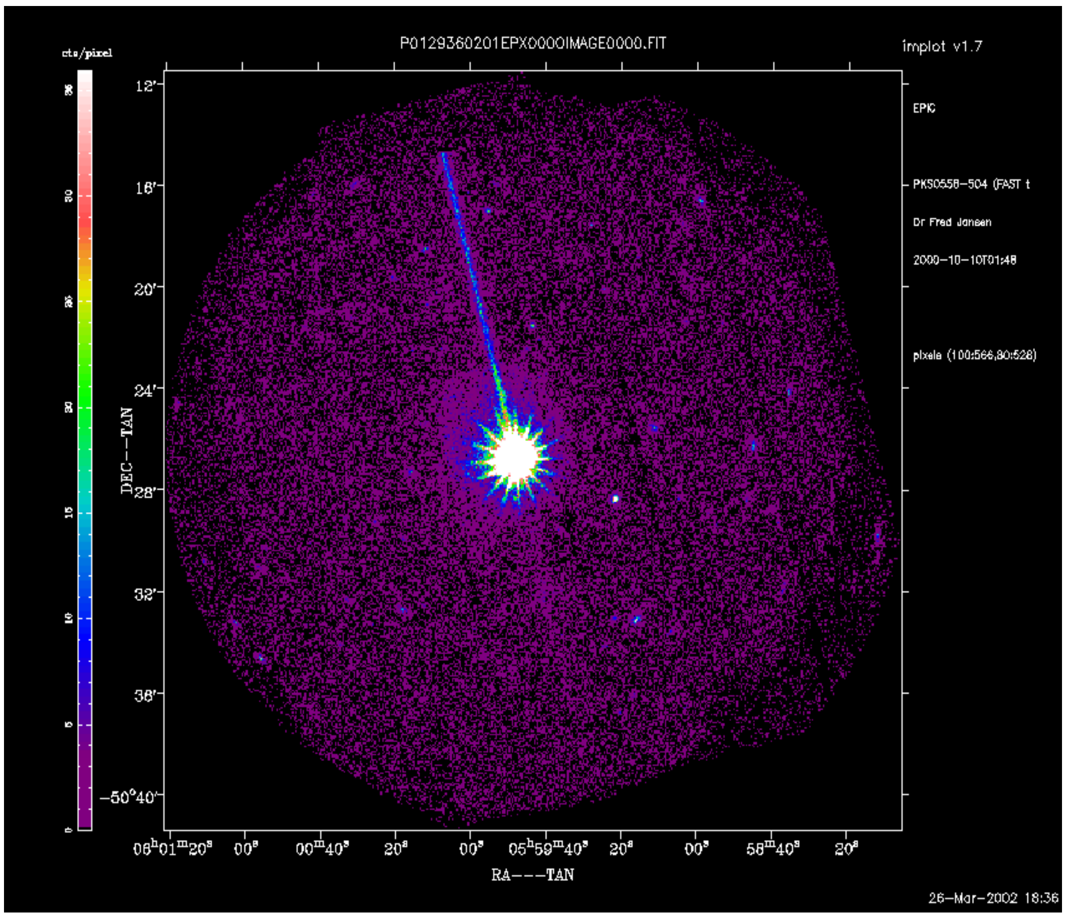

Figure 26: EPIC observation image of PKS 0558–504 in revolution 153

3.1.8 PKS2155-304

PKS2155-304 is one of the main cross calibration objects, observed by XMM-Newton several times (also in conjunction with Chandra). The observation used for this validation report took place in revolution 362, end of November 2001. As the observation configuration shows (Fig. 27) it lasted for more than 92 ksec, including several EPIC MOS exposures in Small Window mode, and two exposures of EPIC PN in Timing and Small Window modes, respectively. RGS1 and RGS2 single exposures covering the entire observation time and several OM exposures using the V, B and U filters complete the observation.

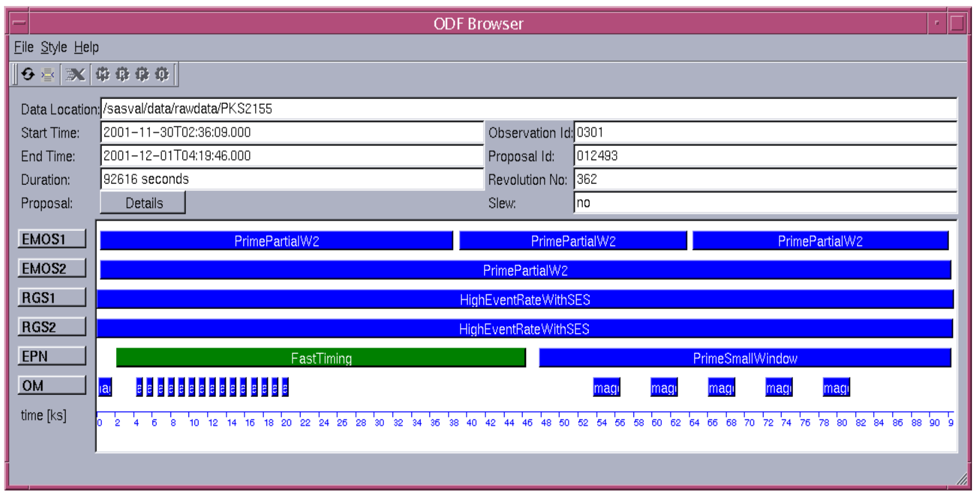

Figure 27: PKS2155-304 observation configuration in rev. 362

3.1.8.1 PPS screening report

```
XMM SSC data-product screening log
Version: 29-Apr-02

Revolution  362
Obs Seq.    0124930301
Target      PKS2155-304
Seq_id      000698


** GENERAL COMMENTS


Bright source in center of EPIC images
Problems:
EPIC source detection

EPIC comments refer, in general, to Energy-band 8.
```

```
** EPIC MOS1


PrimePartialW2 with Thin1 filter (duration 27750.7 s; 27252.5 s in image).
Bright segments of rows/columns in band 8000 (usually 1)
Bright source piled-up in the core
Spurious sources found in bright segments of rows/columns
Spurious sources found in the wings of the bright source

PrimePartialW2 with MEDIUM filter (duration 38249 s; 38000.0 s in image).
Bright segments of rows/columns in band 8000 (usually 1)
Bright source piled-up in the core
Spurious sources found in bright segments of rows/columns
Spurious sources found in the wings of the bright source


PrimePartialW2 with THICK filter (duration 24650 s; 24481.9 s in image).
Bright segments of rows/columns in band 8000 (usually 1)
Bright source piled-up in the core
Spurious sources found in bright segments of rows/columns


** EPIC MOS2


PrimePartialW2 with Medium filter (duration 92018.8 s; 91546.4 s in image).
High background not totally screened in images
Bright segments of rows/columns in band 8000 (usually 1)
Spurious sources found in bright segments of rows/columns
Spurious sources found in the wings of the bright source


** EPIC PN


PrimeSmallWindow with Medium filter (duration 44304.7 s; 41750.4 s in image).


**  RGS1, RGS2


RGS1:
CCD 7 missing
Spatial map: 1 extraction regions
(bright spectrum visible)
Orders image: Bright spectrum visible within 1st and 2nd order
Spectrum plots: Bright spectra (mostly continuum)
RGS2:
```

```
CCD 4 missing
Comments to spectra as RGS1


** OM


15 exposures (5 with Filter  V ; 800 s duration; 5 with Filter  U; 800 s duration; 5 with Filter  B; 800 s duration)
Readout streaks
Ghost rings
Scattered light features
Dark spots (reduced response - 'holes')
Source detection problems:
Few sources missing
Spurious sources in readout streaks


** Catalogue cross-correlation products


Bright EPIC source not present in catalogs
Catalogue positions offset from the XMM source positions
Bright ROSAT and EPIC sources match
```

3.1.8.2 Pipeline Products results

The whole data set product is considered fully acceptable. Fig. 28 shows the combination of all EPIC imaging exposures, as derived by PPS. The RGS1 orders image (Fig. 29) shows also a very clear signature of the third order dispersion. The corresponding subtracted and background spectra of first and second order are shown in the following figure (Fig. 30). The OM composed image of all V-filter exposures is shown in Fig. 31.

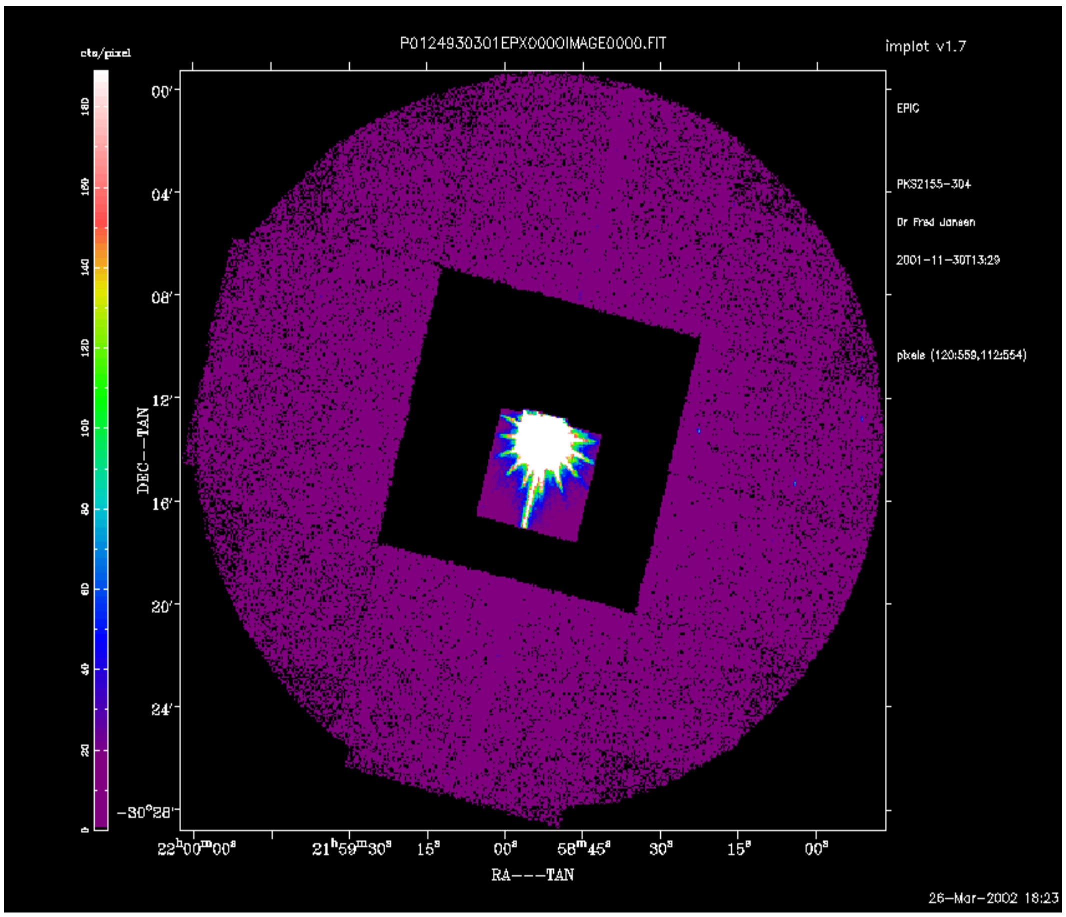

Figure 28: EPIC combined image of PKS2155-304

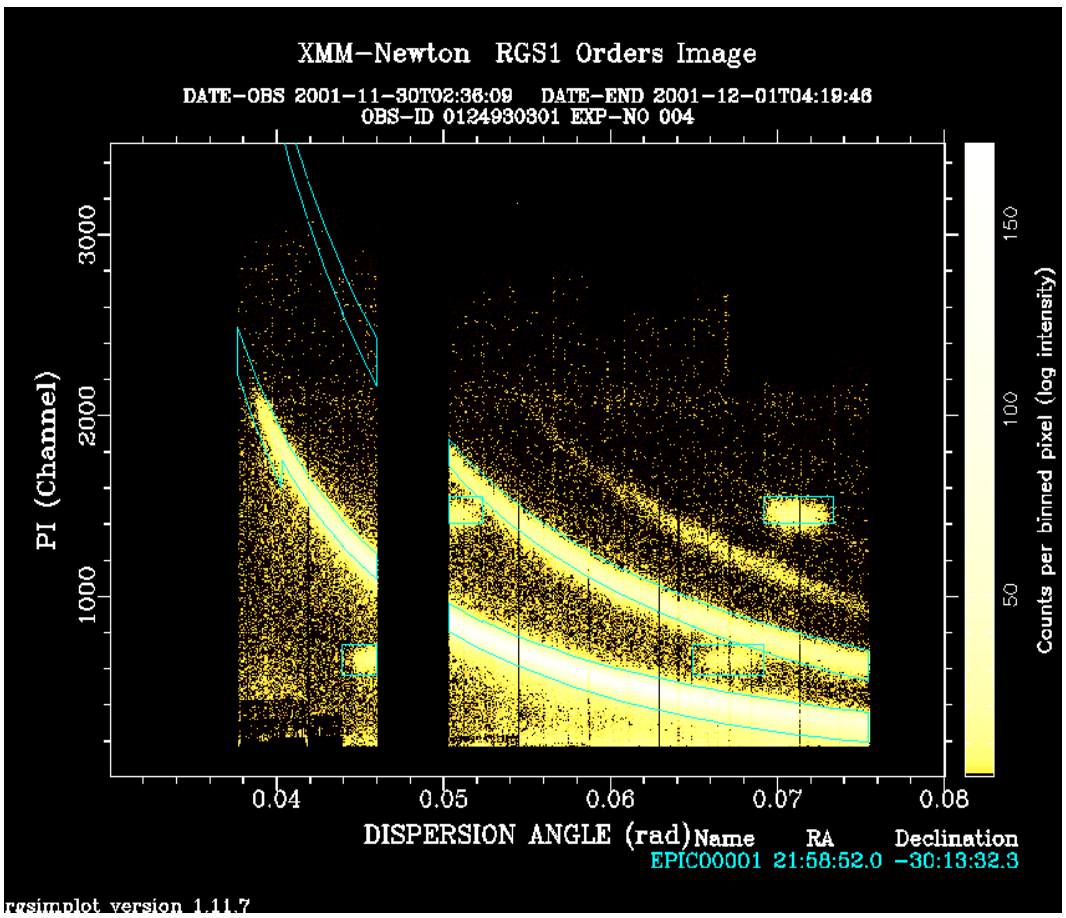

Figure 29: RGS1 order image of PKS2155-304

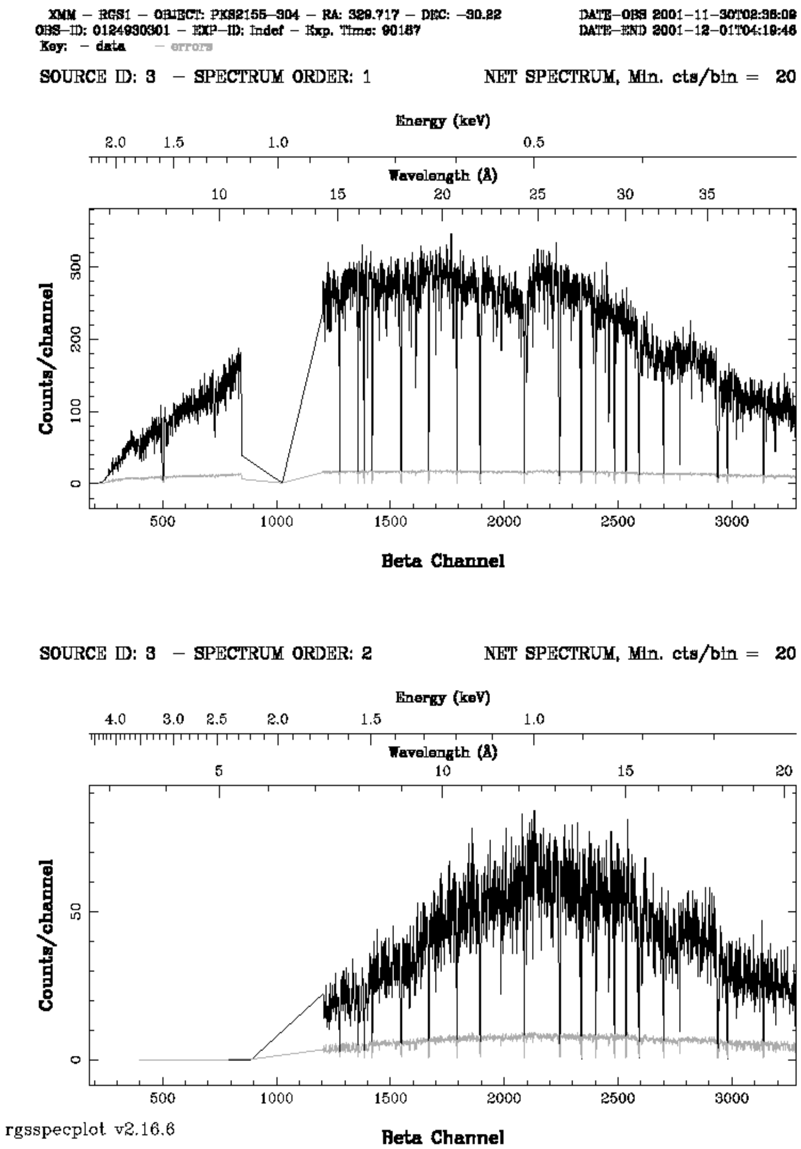

Figure 30: PKS2155-304: RGS1 first and second order subtracted spectra

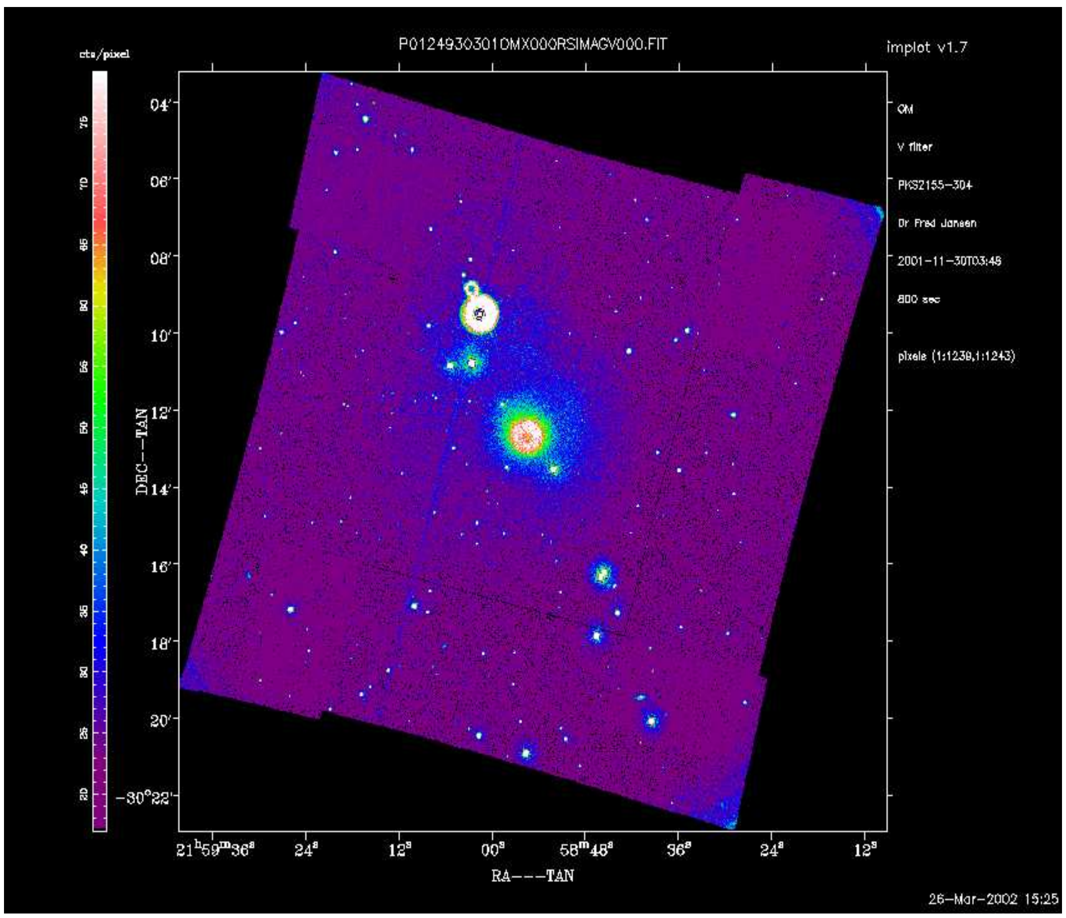

Figure 31: PKS2155-304: OM combined image with the V-filter

3.1.9 XTE J1650500

The stellar black hole XTE J1650500, located on the sky position ($\alpha_{2000} = 16^h50^m1^s.0$, $\delta_{2000} = -49°57'45".0$) was observed during revolution 323 on September 13, 2001, for 25 ksec approximately.

Fig. 32 shows the observation configuration (obtained using *odfbrowser*).

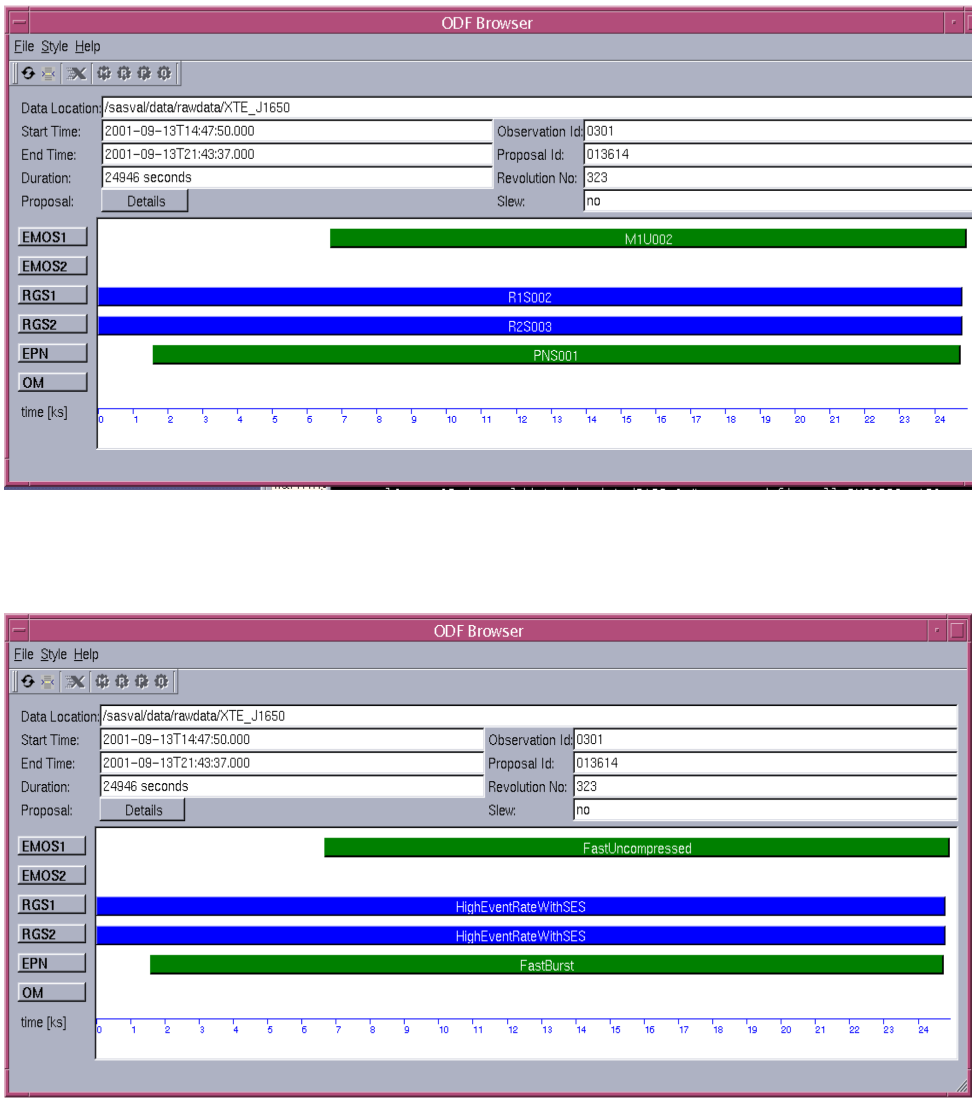

Figure 32: XTE J1650-500 observation configuration

3.1.9.1 PPS screening report

```
XMM SSC data-product screening log
Version: 26-Apr-02

Revolution  323
Obs Seq.    0136140301
```

```
Target      XTE J1650-500
Seq_id      000696


** GENERAL COMMENTS


MOS2 not active
OM not active
Extended bright source in center of EPIC images
Problems:
EPIC source detection
Many useless crosscorrelation products

EPIC comments refer, in general, to Energy-band 8.



** EPIC MOS1


FastUncompressed with Thick filter (duration 18229.8 s 16788.3 s;in image).
The diffraction of the bright source on the RGA generates a spike
High background not screened in images
Flaring activity at end of exposure
Bright segments of rows/columns in band 1
Bright pixels in band 1
Spurious sources associated with extended emission
Spurious sources found in the wings of the bright source
Spurious sources found in diffraction spike
Spurious sources found in bright segments of rows/columns



** EPIC MOS2

Not active. No products


** EPIC PN

FastBurst with Thin1 filter (duration 23200.4 s)


**  RGS1, RGS2


RGS1:
CCD 7 missing
Spatial map: extraction region in center
Spatial map: 1 extraction regions
(bright spectrum visible)
```

```
Orders image: Bright spectrum visible within 1st and 2nd order
Spectrum plots: Bright spectra (mostly continuum)
RGS2:
CCD 4 missing
Comments to spectra as RGS1


** OM


Not active. No products


** Catalogue cross-correlation products


ROSAT image with very short exposure
Bright EPIC source not detected by ROSAT
Many useless correlation products due to spurious sources in EPIC source list
```

3.1.9.2 Pipeline Products results

EPIC MOS2 was not active during this observation, MOS1 was in Timing Mode and PN in Burst Mode. The interactive results obtained with the latter are reported under section 4.4.

Fig. 33, containing the RGS2 order image, shows the enormous amount of photons collected by XMM-Newton during this observation, so that very clear signatures of up to the fifth order can be seen. The corresponding first and second order subtracted spectra, containing mostly continuum, are shown in Fig. 34.

All the main products obtained with the pipeline are considered acceptable.

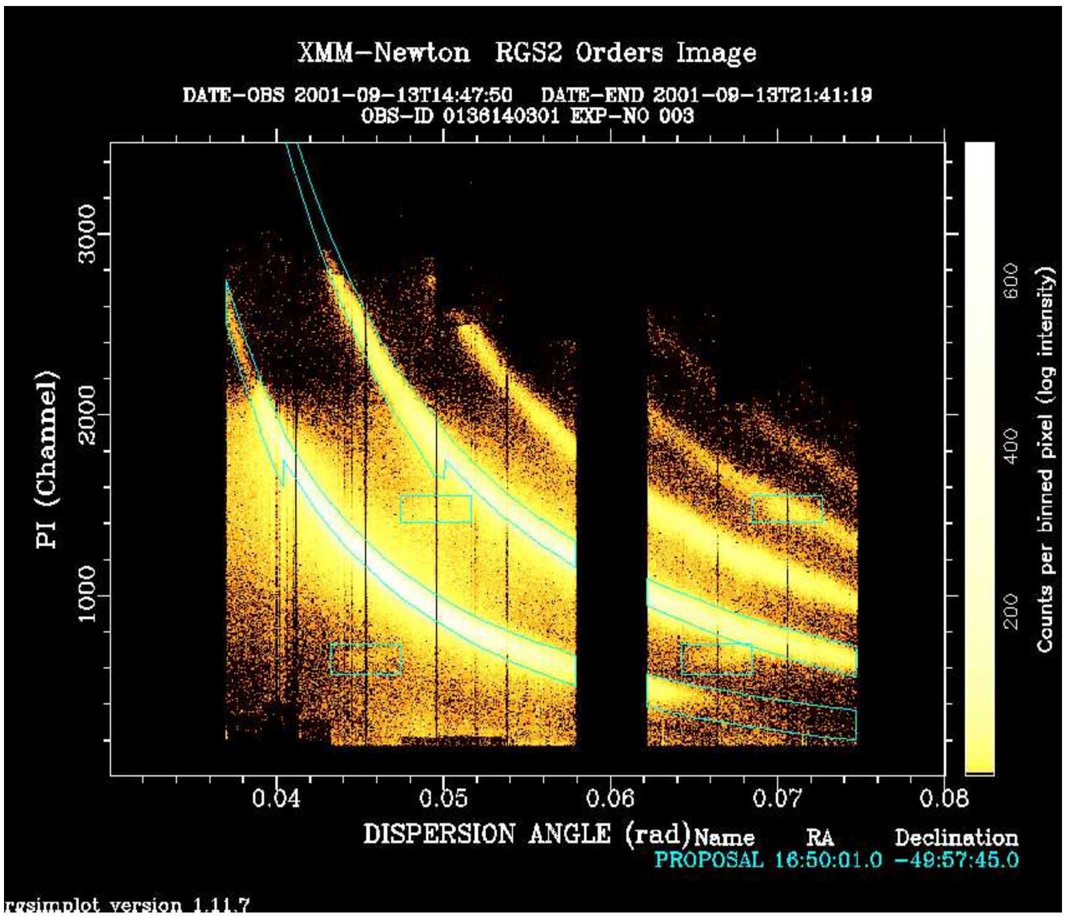

Figure 33: RGS2 order image of XTE J1650500

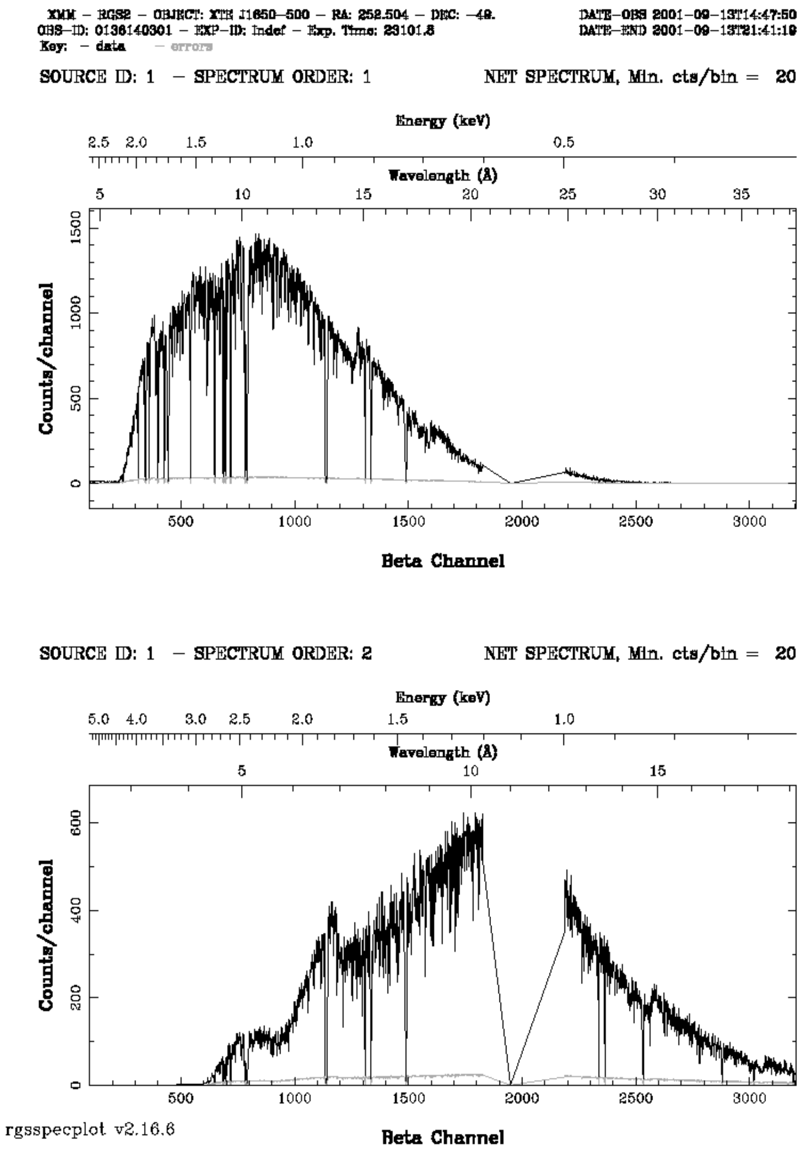

Figure 34: RGS2 first and second order subtracted spectra of XTE J1650500

4 Interactive Analysis Results

4.1 EPIC astrometry

The relative and absolute astrometry on the Lockmann Hole observation in revolution 70 has been revisited in this analysis.

The sky coordinates of the sources are compared in figure 35. Only the 8 brigthest sources common to MOS1, MOS2 and PN could be used to compare celestial coordinates, and for the faintest ones used, the uncertainty on the X-ray position is dominated by the statistical accuracy of the measurements of about 1 arcsec.

The agreement between MOS1 and MOS2 positions is very good across the whole field of view with a typical rms fluctuations of about 1 arcsec.

On the other hand, there is evidences for a shift of about 1-2 arcsec between PN and MOS1, but the validity of this offset is limited by the small number of the sources used.

The coordinates returned by PN were compared to the (most likely) optical counterparts coordinates, from Lehmann et al. (2001). Most of the sources are point-like AGNs that were already detected in the ROSAT deep survey. More sources (18) could be used this time for this cross-correlation exercice.

The difference between PN and optical coordinates is plotted in Fig. 36, sources up to 12 arcmin off-axis were used. A shift from the PN reference frame to the absolute frame of about 3 arcsec is evident, compatible with the findings of Tedds & Watson (2001). It is due to the limited accuracy of the attitude reconstruction from the star tracker.

However once this shift is applied the difference of the PN sky coordinates to absolute is only **1.1 arcsec** (root mean square). This is a remarkable result considering the pixel size of the PN detector (4.1").

Besides, this 1 arcsec error is an upper limit because:

1. the optical coordinates have a limited accuracy (about 0.3 arcsec)
2. the uncertainty of the coordinates returned by *edetect_chain* for the faintest PN sources used is about 0.1-0.2 arcsec

This demonstrates the very good accuracy of the EPIC-PN plate-scale calibration.

4.1.0.3 Conclusions

1. MOS1 and MOS2 relative astrometry accuracy is about 1" across the field-of-view, *based on a limited number of sources.*
2. The EPIC-PN plate scale is excellent over the whole field-of-view, (1" r.m.s. relative astrometry)

4.1.0.4 EPIC sources photometry

The SAS source detection tasks include the calculation of fluxes for each source and energy band, which are written into the source lists. The complex nature of the dependence on parameters settings makes a study of accuracies in this respect outside the scope of this validation and should be done in the framework of a dedicated calibration report.

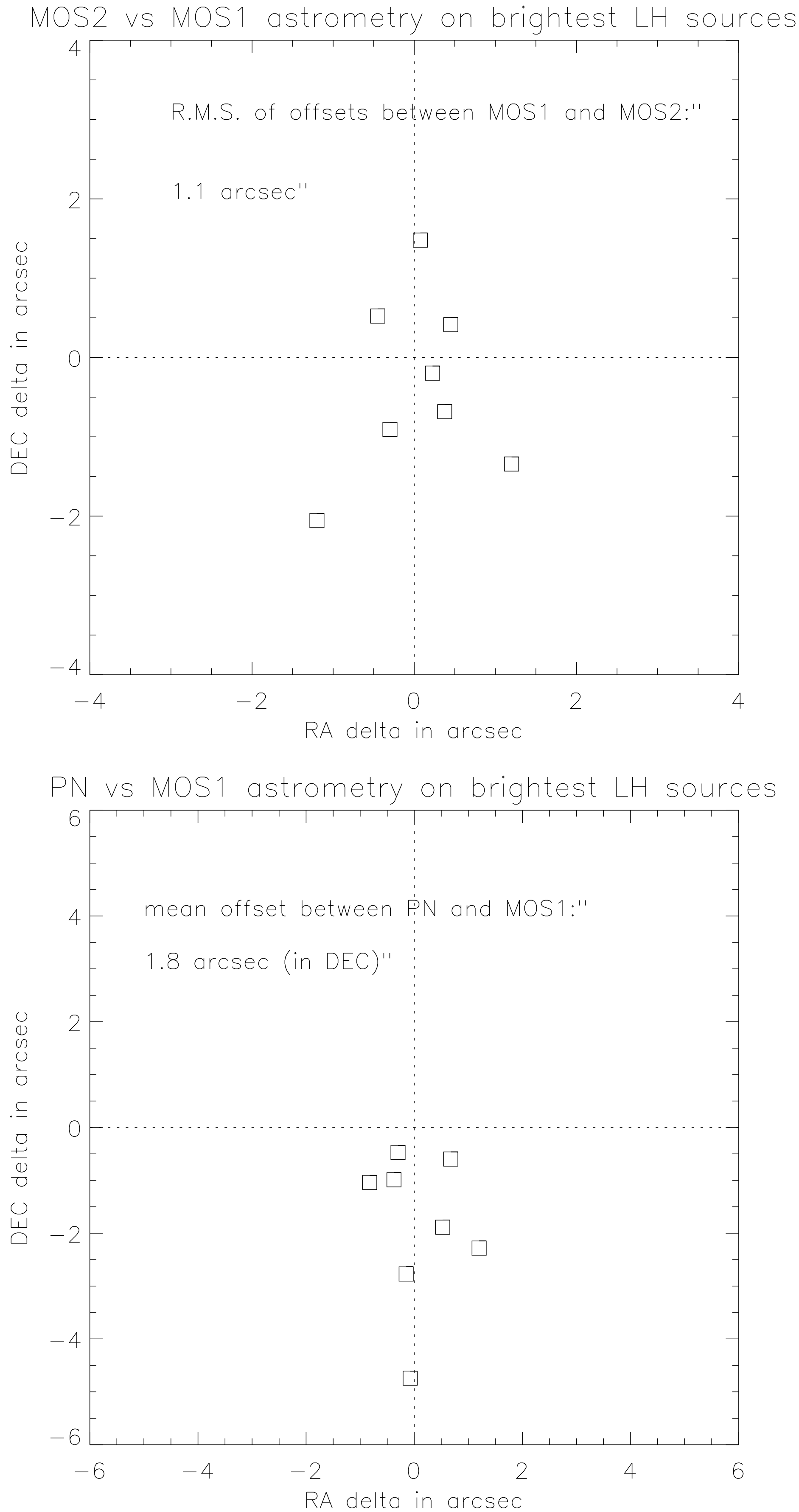

Figure 35: Comparison of sky coordinates between 1) MOS1 and MOS2, 2) PN and MOS1

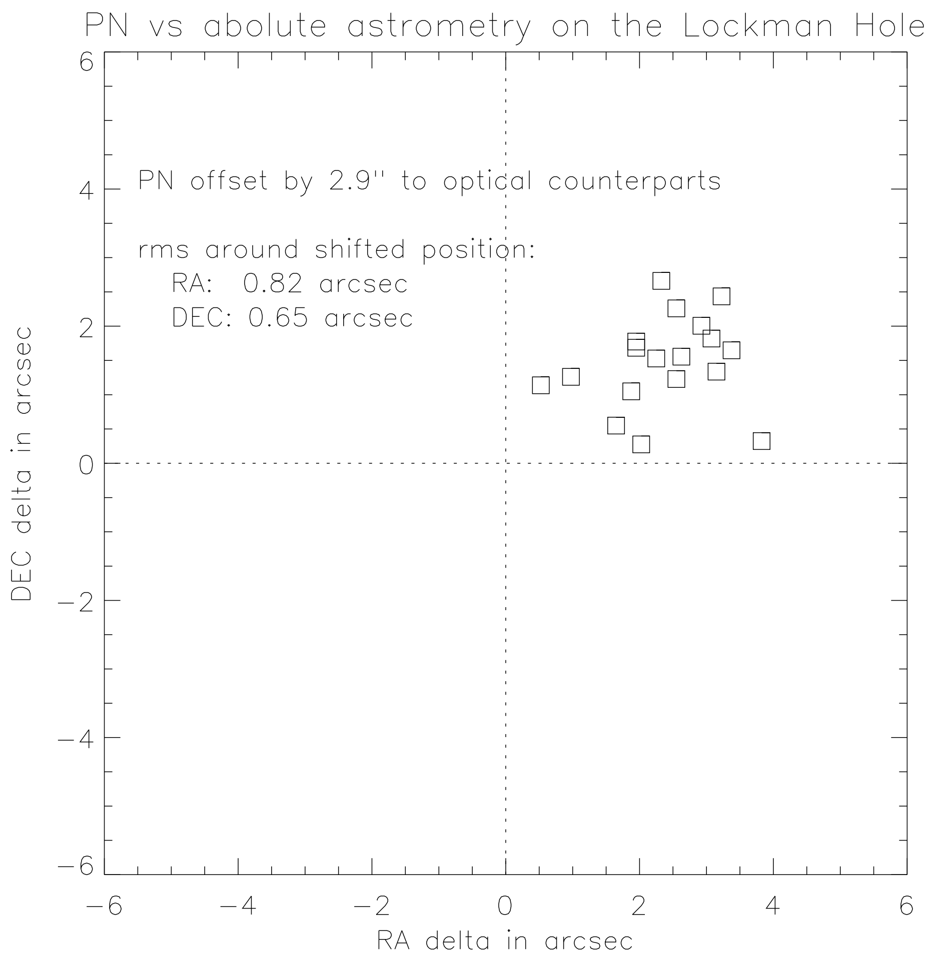

Figure 36: Difference of PN sky coordinates to absolute (optical counterparts, from Lehmann et al., 2001)

4.2 Quality of EPIC spectral fitting

Response matrices for EPIC spectral fitting can be obtained with SAS v5.3.x in three ways:

1. generating a redistribution matrix via the SAS task *rmfgen* and an effective area vector via the SAS task *arfgen*
2. generating an effective area vector via the SAS task *arfgen*, using a standard redistribution matrix (available through the web page `http://xmm.vilspa.esa.es/ccf`) as input to *arfgen* to calculate consistently the energy grids
3. using a standard response matrix file, again available through the web page `http://xmm.vilspa.esa.es/ccf`

We remind that a "response file" (extension `*.rsp`) is a ready-made combination of a redistribution matrix (extension `*.rmf`) and an ancillary file vector (extension `*.arf`). For more details we advise the reader to look at the HEASARC OGIP memos, such as
`http://heasarc.gsfc.nasa.gov/docs/heasarc/caldb/docs/memos/cal_gen_92_002/cal_gen_92_002.html`.

All the above outlined methods are available and fully functional for all EPIC cameras with SAS v.5.3.

4.2.1 The G21.5-09 case

The X-ray spectrum of the Crab-like SuperNova Remnant (SNR) G21.5-0.9 (Warwick et al. 2001) is well described by a strongly absorbed (column density, $N_H \sim 2 \times 10^{22}$ cm^{-2}) power-law. At o-th order, it can be characterized through 3 quantities only: N_H, the photon index Γ and the model normalization. This source is therefore particularly well-suited to compare the performances of the response matrices above 1 keV.

In the following, uncertainties are quoted at the 90% confidence level for one interesting parameter, and each data point corresponds to a signal-to-noise ratio >3.

The XMM-Newton observation discussed in this report was performed on April 7, 2000. The EPIC cameras were operating in Full Frame (MOS), and Extended Full Frame (PN) mode, respectively. The source was on-axis. Source spectra have been extracted from circular regions of 1' radius around the centroid of the SNR. Background spectra have been extracted from an annulus of 3.15' to 4.6' radius. The source spectra have been rebinned in order to have at least 50 counts in each spectral bin and to oversample the instrumental energy resolution by a factor not higher than 3. The spectra have been fit in the 0.3-12 keV and 0.1-15 keV energy bands for MOS and PN, respectively. A detector map has been extracted for each EPIC camera and used as an input to *arfgen*, since the centroid of the nebula is surrounded by an extended halo. The model employed is a simple power-law with photoelectric absorption.

Above 2 keV, the residuals (expressed in terms of data/model ratio), are generally within ±5% (the scatter is largely dominated by statistical uncertainties below this level). As shown in Fig. 37, "waves" in the residuals of the order ±10% are present around the gold edge ($E \simeq$ 2.2 keV) in the MOS2 and, at a smaller level, in the MOS1 and PN. In such a strongly absorbed source small uncertainties in the knowledge of the redistribution function may have a significant impact on the quality of the spectral fitting below 1 keV, where the counts decrease by a factor $\simeq 100$ with respect to the energy band around 2 keV. This most likely explains the soft excesses observed in the MOS2 and PN residuals below $\simeq$1 keV, and of the count deficit in the MOS1 below $\simeq$0.7 keV.

No iron line feature is measured in either spectrum. In Tab. 2 the upper limits on the equivalent width of an unresolved line corresponding to K_α transitions of neutral, He-like and H-like iron are shown. They correspond to fluxes in the range 10^{-6}–10^{-5} photons cm^{-2} s^{-1}.

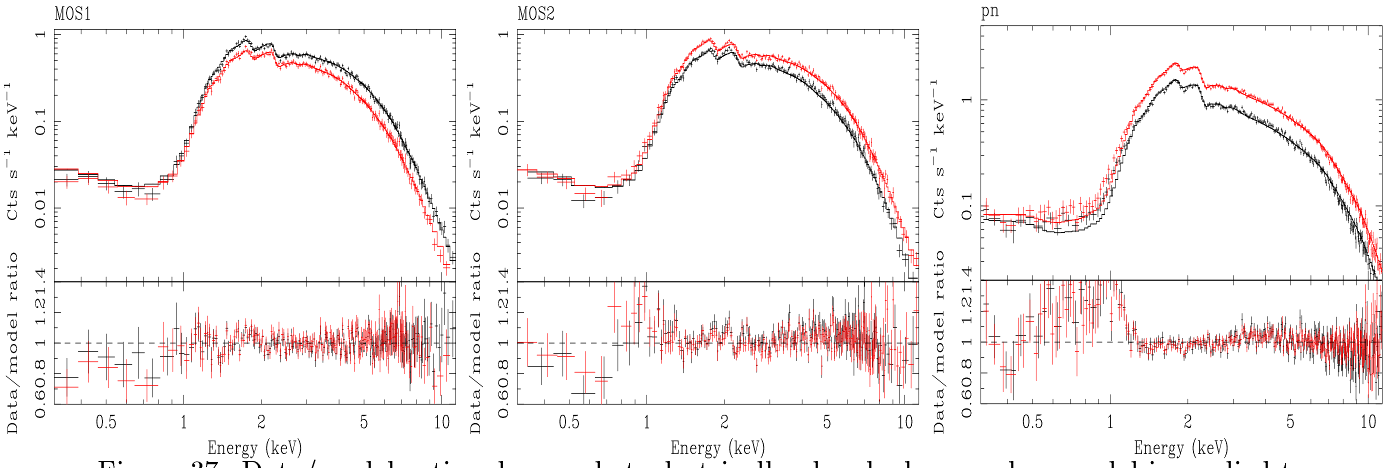

Figure 37: Data/model ratio when a photoelectrically absorbed power-law model is applied to the G21.5-0.9 spectra of MOS1 (*left panel*), MOS2 (*central panel*) and PN (*right panel*). *Black crosses* correspond to the spectra extracted from single and double events, *red crosses* to spectra extracted from singles events in the MOS1 plot and the other way around in the other two plots. The fit parameter values used for the figures are given in Tab. 3.

Transition	MOS1	MOS2	PN
Neutral ($E = 6.4$ keV)	27	14	7
He-like ($E = 6.76$ keV)	37	8	3
H-like ($E = 6.9$ keV)	33	27	3

Table 2: 90% upper limits on the equivalent width of an unresolved iron line of centroid energy E in the G21.5-0.9 EPIC spectra

Fig. 37, together with Tab. 3, presents a comparison between spectra extracted with singles and doubles events (*black crosses*) and with single events only (*red crosses*). The residuals patterns are fully indistinguishable, and the corresponding best-fit parameters are fully consistent within the statistical uncertainties.

As from SAS v5.3, "standard" response matrices are not longer needed for most of the EPIC modes (including the ones used in this observation), because *rmf/arfgen* exactly reproduce the response matrices produced by the EPIC Instrument Team. Still, it is possible to download from the SOC calibration web site redistribution matrices, which may be used as input to *arfgen* (via `withrmfset=yes` and `rmfset=${redistribution matrix file}`). This procedure yields a substantial saving of computation time, because each *rmfgen* run can last up to several hours. The results obtained following the two procedures are virtually identical, as shown in Tab. 3.

In Fig. 38 a comparison between the iso-χ^2 contour plots of the 3 quantities characterizing the overall X-ray spectrum of G21.5-0.9 is shown. The absorbing column density measured by the pn is $\Delta N_H \simeq 0.1 \times 10^{22}$ cm^{-2} lower than by the MOS cameras. Spectral indices in the 2–10 keV band are consistent within the statistical uncertainties, with a slight trend for the face-values to decrease gradually by $\Delta\Gamma \simeq$0.07 from PN to MOS1 to MOS2. The 2–10 keV PN flux is $\simeq$ 6% lower than in the MOS1 and $\simeq$ 3% lower than in the MOS2 camera. Although the difference is still not negligible, this represents a substantial improvement with respect to SAS v5.1.

Scenario	Γ	N_H (10^{22} cm^{-2})	2-10 keV flux (10^{-11} erg cm^{-2} s^{-1})
MOS1			
singles	$1.89\pm^{0.03}_{0.04}$	$2.35\pm^{0.04}_{0.05}$	6.06 ± 0.06
singles+doubles	$1.85\pm^{0.02}_{0.03}$	2.30 ± 0.04	$6.03\pm^{0.06}_{0.05}$
singles+doubles†	$1.85\pm^{0.03}_{0.02}$	2.30 ± 0.04	$6.03\pm^{0.06}_{0.05}$
MOS2			
singles	1.92 ± 0.03	2.30 ± 0.05	5.94 ± 0.06
singles+doubles	$1.91\pm^{0.02}_{0.03}$	2.28 ± 0.04	5.84 ± 0.05
singles+doubles†	$1.91\pm^{0.02}_{0.03}$	2.28 ± 0.04	5.84 ± 0.05
PN			
singles	1.849 ± 0.018	$2.20\pm^{0.04}_{0.03}$	5.44 ± 0.04
singles+doubles	1.820 ± 0.015	$2.18\pm^{0.02}_{0.03}$	5.41 ± 0.03
singles+doubles†	1.820 ± 0.015	$2.18\pm^{0.02}_{0.03}$	5.41 ± 0.03

†standard redistribution matrices as input to *arfgen*

Table 3: G21.5-0.9 observation best-fit parameters. Errors are at the 90% confidence level for one interesting parameter.

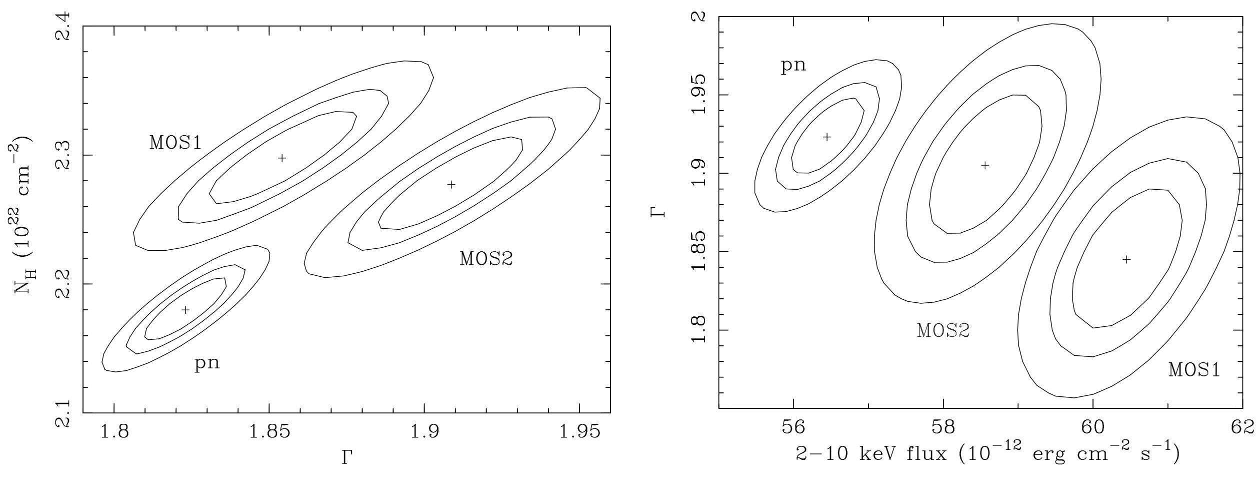

Figure 38: Iso-χ^2 contour plots for Γ versus N_H (*left panel*) and Γ versus the 2–10 keV flux (*right panel*) for the best-fit models applied to the MOS1, MOS2 and PN spectra of G21.5-0.9. In the former case, the model is applied to the whole sensitive bandpass of each EPIC camera; in the latter only in the 2–10 keV band. Contours correspond to the 68%, 90% and 99% confidence levels for two interesting parameters

4.2.2 PKS0558-504

Analysis of PKS0558-504 is based on EPIC observations obtained in revolutions 84 and 153: In both revolutions a PN exposure was performed in Small Window mode and MOS1 and MOS2 in Large Window mode. In rev.84 the MEDIUM filter was used for all EPIC cameras, whereas the THIN filter was used in revolution 153.

In the rev.84 EPIC exposures, the data needed to be cleaned for high flaring background (accepting only time intervals with less than 1 cts/s in the energy range above 10 keV for PN and 0.35 cts/s for MOS1 and MOS2, respectively), which reduces the available exposure ontime from 13.6 to 8.3 ks (PN) and from 13.9 to 11.9 ks (MOS1) and 11.4 ks (MOS2). The rev.153 was free of such flaring background and the total 10.7 ks (PN) and 7.9 ks (MOS) could be taken into account.

According to the *epatplot* created pattern statistics, the EPIC window mode observations are not significantly affected by pile-up.

The PN Full Frame mode exposures also taken in revolutions 84 and 153 are likely to be affected by pile-up, and therefore were excluded from this report.

Spectra have been extracted from circular areas centered on PKS0558-504 and have been grouped with a minimum number of 25 counts per channel and a factor of three by which to oversample the EPIC energy resolution. Standard quality flag and pattern selections have been adopted: `(FLAG==0) && (PATTERN<=4)` (PN) and `(FLAG==0) && (PATTERN<=12)` (MOS). Background spectra have been extracted from source-free annuli around PKS0558-504. Response matrices have been generated with *rmfgen* and *arfgen*, with `detmaptype=psf`.

The spectra have been fit with a model constituted of a power-law and two blackbodies (*baseline model*; the third blackbody envisaged by O'Brien et al. 2001 is actually not required by the fit of this dataset). The power-law component dominates above 2 keV, the blackbodies account for the bulk of the prominent soft X-ray excess. The best-fit parameters and results are summarized in Tab. 4.

Instrument	Γ	kT^1_{BB} (eV)	N^1_{BB} (10^{-5})	kT^2_{BB} (eV)	N^2_{BB} (10^{-5})	F (0.1-2 keV) (10^{-11} erg cm^{-2} s^{-1})	F (2–10 keV)	χ^2/ dof
				Rev.84				
PN	$1.72^{+0.05}_{-0.06}$	137 ± 2	21.2 ± 0.9	348^{+11}_{-14}	$7.0^{+0.4}_{-0.5}$	3.29	1.14	303/210
MOS1	$1.45^{+0.09}_{-0.13}$	117 ± 2	$20.2^{+0.6}_{-0.8}$	360 ± 16	$7.5^{+0.8}_{-0.7}$	2.68	1.01	415/218
MOS2	$1.46^{+0.09}_{-0.08}$	118^{+1}_{-2}	$20.2^{+0.7}_{-0.5}$	337^{+15}_{-17}	$7.4^{+0.8}_{-0.9}$	2.73	1.04	416/215
				Rev.153				
pn	$1.66^{+0.07}_{-0.10}$	146^{+1}_{-2}	$20.9^{+0.7}_{-0.6}$	390 ± 13	$7.2^{+0.3}_{-0.4}$	3.11	1.20	434/216
MOS1	1.49 ± 0.08	123^{+2}_{-3}	18.3 ± 0.8	363^{+12}_{-17}	$8.5^{+0.9}_{-1.1}$	2.78	1.26	308/172
MOS2	$1.51^{+0.09}_{-0.10}$	129 ± 2	$19.1^{+0.7}_{-1.0}$	412^{+20}_{-19}	$8.2^{+1.0}_{-0.9}$	2.74	1.22	273/175

Table 4: PKS0558-504 best-fit parameters for PN Small Window mode and MOS Large Window mode observations in rev.84 (MEDIUM filter) and rev.153 (THIN filter), respectively. kT and N are the temperature and the normalization of the blackbody components. F is the measured flux

In Fig. 39, 40 and 40 the ratios of the data against the best-fit model are shown, when the baseline model is applied to the PN Small Window mode and MOS1 and MOS2 Large Window mode spectra obtained in rev.84 and 153.

The fits for the individual EPIC cameras (PN, MOS1 and MOS2) agree well between these two revolutions (cf. Table 4) which holds also true for a comparison of the MOS1 with the MOS2 camera. However, there exist significant differences in the fit parameters between EPIC PN on one side and the MOS cameras on the other side (esp. in respect to the fitted powerlaw index and the temperatures of the two black-body components). Found flux differences between PN

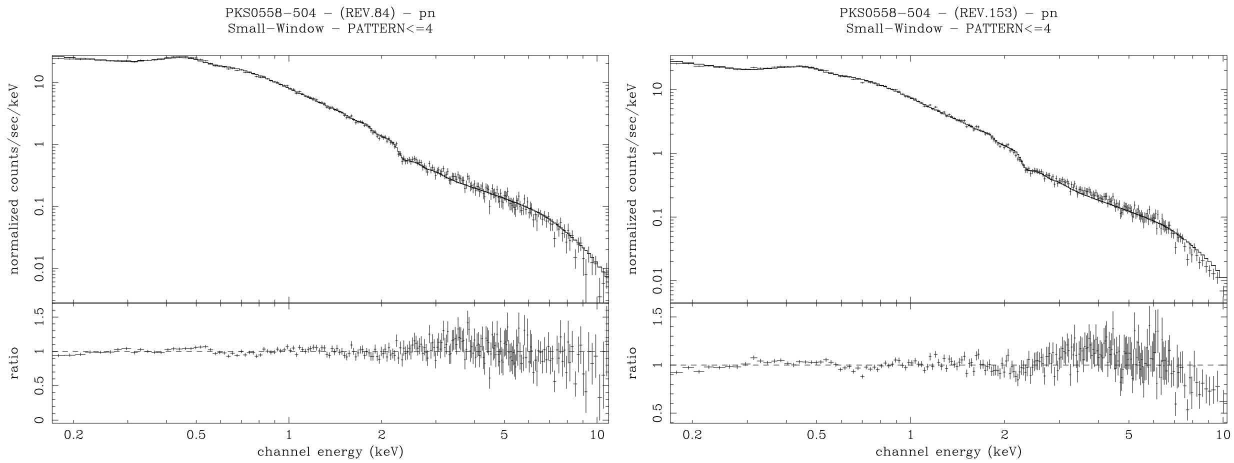

Figure 39: PKS0558-504 PN spectra (*upper panels*) and residuals in units of data/model ratio (*lower panels*) when the baseline model is applied to the spectra of the Small Window exposure in rev.84 (*left*) and to the exposure in rev.153 (*right*).

and MOSs are of the order of 17% in the soft energy range 0.1 - 2 keV (where highest fit residuals are found - cf. Fig. 42), whereas fluxes agree within 5% in the energy band 2 - 10 keV.

In addition a simultaneous fit of MOS1, MOS2 and PN rev. 153 data using the same model was performed, between 0.2 and 10. keV. The EPIC MOS data were taken using Large Window mode with the THIN filter. Standard quality flag and pattern selections have been adopted but no special binning was performed. The results (Fig. 42) show a discrepance in the cross calibration of the EPIC instruments for this mode and filter of up to 20%, in the range [0.5-1.] keV, while otherwise a general good agreement is achieved. For completion the best fit parameters obtained are given in table 5. The results of simultaneous fitting of these data including also RGS data are presented in section 4.5.

Γ	kT^1_{BB} (eV)	N^1_{BB} (10^{-5})	kT^2_{BB} (eV)	N^2_{BB} (10^{-5})	χ^2/ dof
1.71 ± 0.03	135 ± 1	18.2 ± 0.8	369 ± 7	6.8 ± 0.6	2030/554

Table 5: PKS0558-504 best-fit parameters of simultaneous MOS1, MOS2 and PN data fitting

The cross calibration discrepancies make further analysis work (testing models and parameters) in the framework of this validation report unnecessary. However, to show that the problem is located fundamentally in the energy range below 1.3 keV, we have added galactic absorption to the model (nH=4.4E-24), which makes possible to fit better the high energy part of the spectra. Fig. 43 shows the simultaneous fit of all three EPIC cameras in this fit.

The existing discrepancies in the cross calibration are one of the main activities of the XMM-Newton cross calibration team, aiming to reduce them to less than 5% in the very near future.

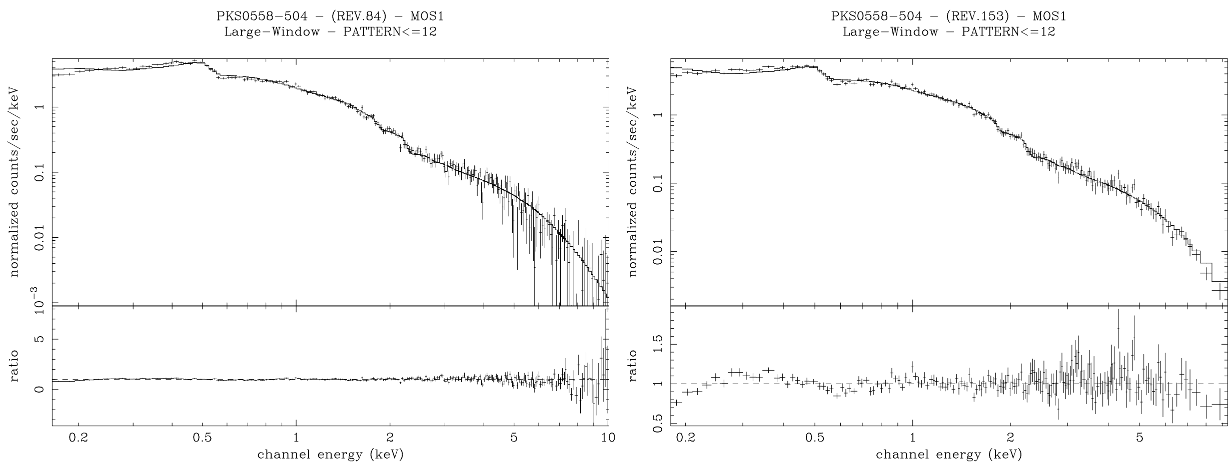

Figure 40: PKS0558-504 MOS1 spectra (*upper panels*) and residuals in units of data/model ratio (*lower panels*) when the baseline model is applied to the spectra of the Large Window exposure in rev.84 (*left*) and to the exposure in rev.153 (*right*).

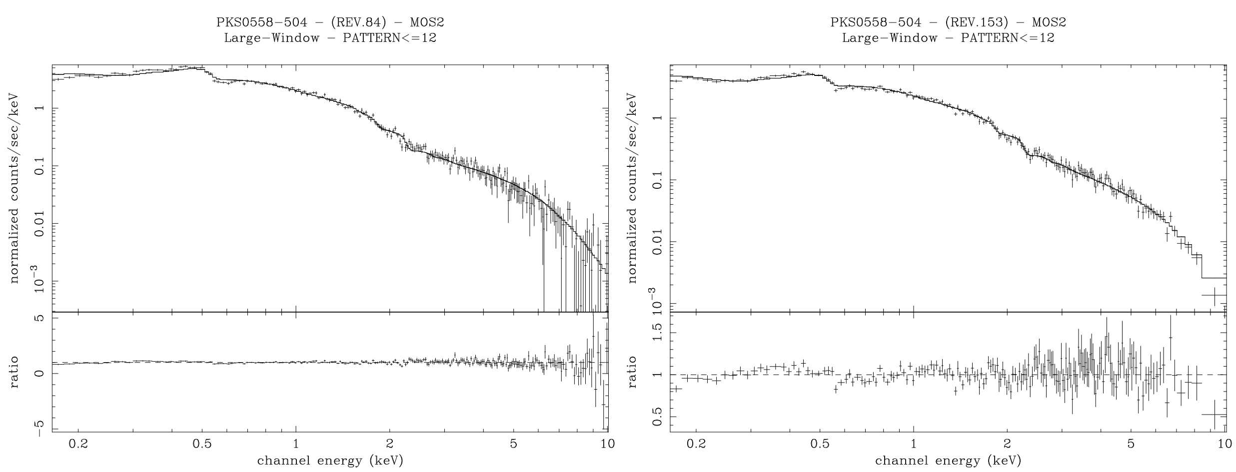

Figure 41: PKS0558-504 MOS2 spectra (*upper panels*) and residuals in units of data/model ratio (*lower panels*) when the baseline model is applied to the spectra of the Large Window exposure in rev.84 (*left*) and to the exposure in rev.153 (*right*).

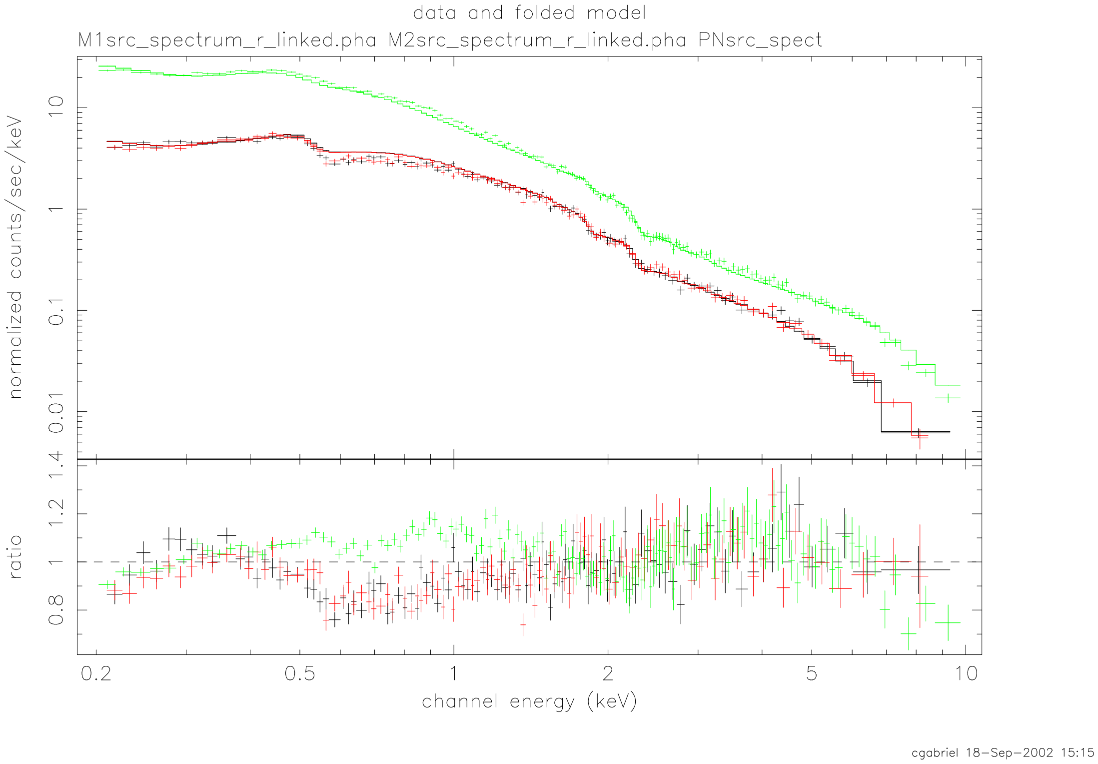

Figure 42: PKS0558-504 PN (green), MOS1 (black) and MOS2 (red) spectra together with residuals in units of data/model ratio (*lower panel*) when the baseline model is applied to the spectra of the Small Window (PN) and Large Window (MOS) exposures of rev.153.

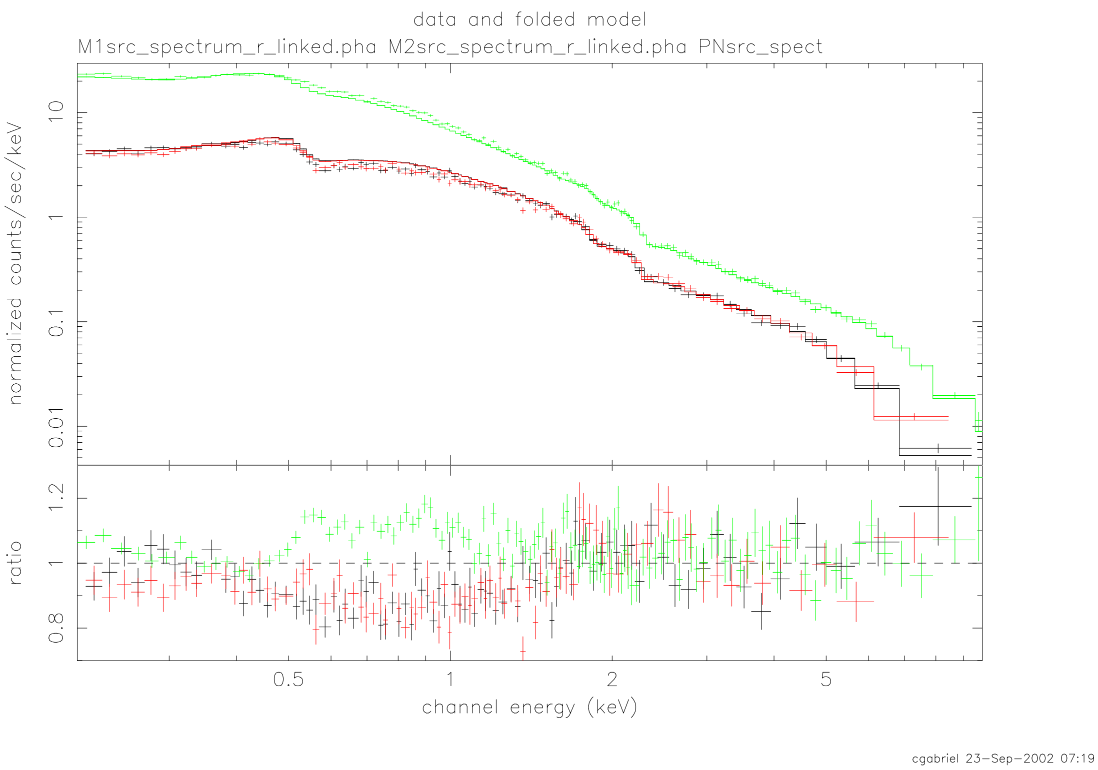

Figure 43: PKS0558-504 PN (green), MOS1 (black) and MOS2 (red) spectra together with residuals in units of data/model ratio (*lower panel*) fitting a power law plus two blackbodies model, including galactic absorption.

4.2.3 PKS 2155-304

The main purposes of using this observation for scientific validation are to:

- verify the correct SAS functionality for PN Timing Mode data;
- ascertain a measure of the spectral data quality of this mode.

Starting point for the validation of the SAS v5.3 interactive analysis is the pipeline produced event list.

The 1-10 keV rate curve is shown in Fig. 44. Note that there is no background subtraction, nor are the time bins exposure corrected as the SAS task required for light curve gti correction, *lccorr*, was not included in the SAS delivery at the time of this validation. This is the reason for the drops seen in the countrate spectrum. However, the background count rate shows no major variation in time implying that the variation in count rate trend should mainly be ascribed to the source, which is known to be highly variable (e.g. Sembay et al. 1993).

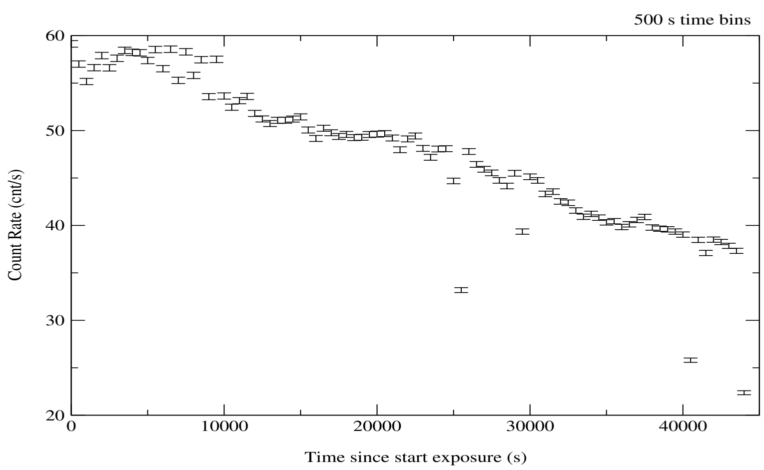

Figure 44: The PKS 2155-304 rate curve in the 1-10 keV band (without background subtraction)

The first 12 ks of the observation were affected by periods of counting mode, a data handling configuration which occurs when the telemetry rate is too high for the available band width. This period has however been included in the spectral analysis.

The SAS task *rmfgen* does not yet support the EPIC PN Timing Mode, hence the latest standard response matrix file (for the corresponding mode and filter), *epn_ti40_sdY9_medium.rsp*, was used for spectral fitting. This file is a combination of the redistribution matrix and ancillary response vector, and requires spectra extracted with single and double events, above a 40 ADU threshold.

The following source and background regions were selected:

source:	((DETX,DETY) IN box(375.612,-111.164,1920.8,76.832,0))
background:	((DETX,DETY) IN box(2693.9,-111.164,344.568,76.832,0)||
	(DETX,DETY) IN box(-1829.78,-111.164,217.168,76.832,0))

Spectra were extracted filtering on PATTERN<=4 (single and double events) and FLAG==0 (e.g. ignoring CCD borders).

An absorbed broken power law provides a reasonable fit in the 0.6-11 keV energy range (see Fig. 45). The best fit parameters are presented in Table 6. This results in an average 2-10 keV flux of $\sim 6.22 \times 10^{-11}$ erg cm^{-2} s^{-1}, hence in this observation PKS 2155-304 is at a medium flux level (e.g. Giommi et al. 1998). The residuals at ~ 2.2 keV are due to current calibration uncertainties regarding the Au edge in telescope effective area. Below 0.5 keV, the PN Timing Mode suffers from high noise.

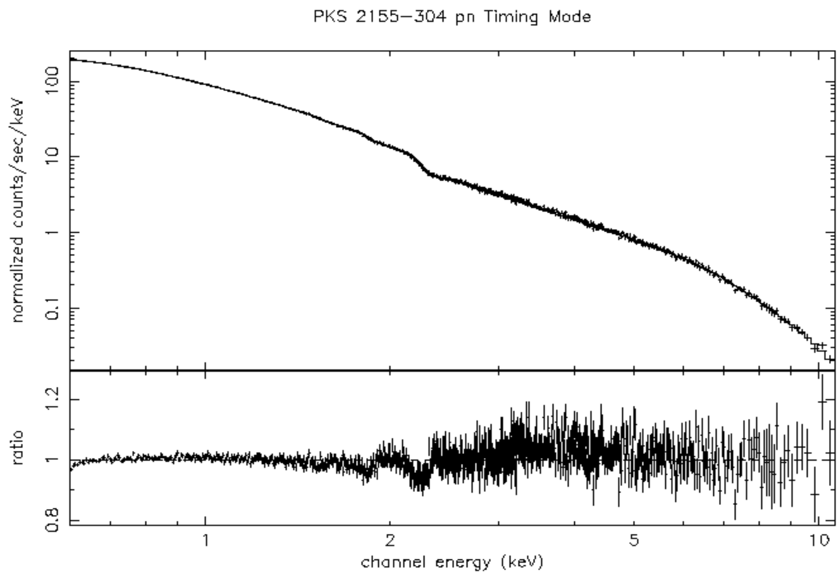

Figure 45: PKS 2155-304 spectrum and best fit data to model ratio

Γ_1	Γ_2	$E_b(keV)$	χ^2/ dof
2.86 ± 0.01	3.09 ± 0.05	5.8 ± 1.0	1367.2/813

Table 6: PKS 2155-304 best-fit parameters assuming an absorbed broken power law

4.3 Her-X1

XMM-Newton observed HER-X1 ($\alpha_{2000} = 16^h 57^m 49^s.80$, $\delta_{2000} = +35°20'32'.6$) , several times. The observation used in this report took place on January 26, 2001, revolution 207, lasting more than 9000 seconds. This validation concentrates only on EPIC pn Timing Mode data, because the MOS Timing mode data can currently not be used, because no response matrices are available for the MOS timing mode.

Spectra have been extracted using single and double events neglecting the events at CCD borders and events lower than 0.5 keV where data should not be used due to the high noise below 0.5 keV in EPIC-pn Timing Mode.

```
((PATTERN .LE. 4 && FLAG==0 && PI .GE. 500))
```

The spectra have been fit with a model constituted by absorption (wabs), a power law, a discblackbody, and four gaussian lines (two of them broad). Several residual features are known to be due to current uncertainties in the calibration.

Fig. 46 shows a plot of Her X1 (data and model) of the best fit to the PN Timing mode spectrum.

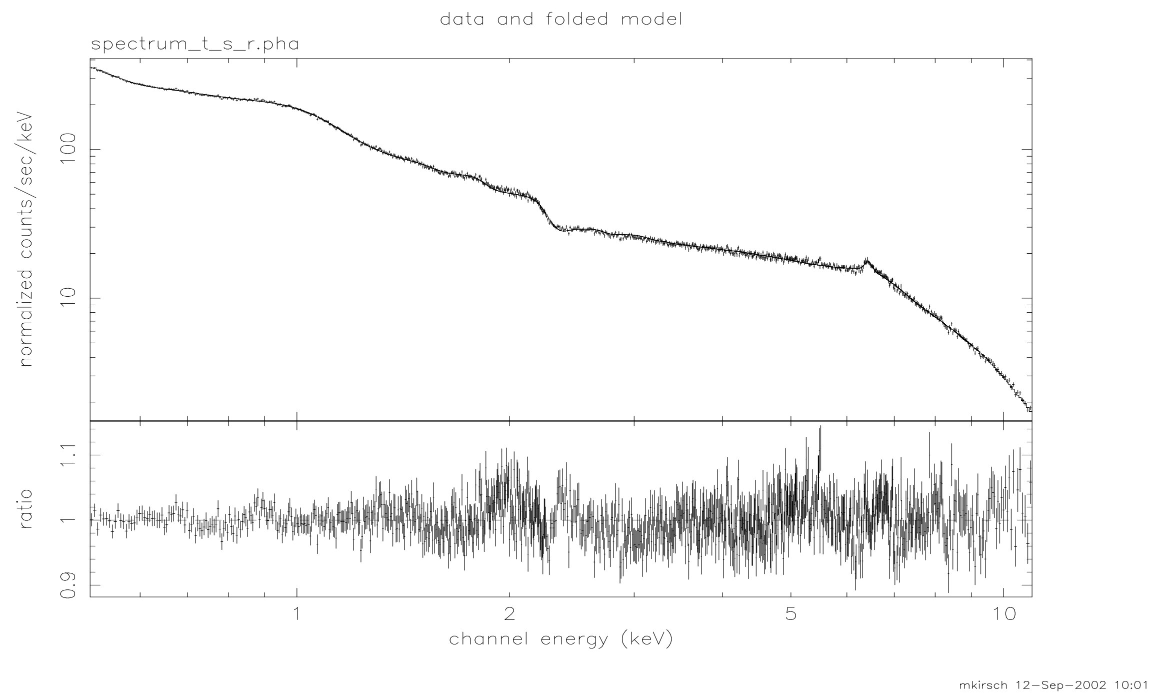

Figure 46: Spectrum of Her-X1 in EPIC PN Timing mode

The best-fit parameters and results are summarized in Tab. 7.

Instrument pn	Γ	Tin (eV)	N_{BB} (10^4)	$LineE$ (keV)	$Sigma$ (keV)	$LineE$ (keV)	$Sigma$ (keV)
	$0.8641\pm^{0.0048}_{0.0048}$	$190.\pm^{36}_{36}$	$1.2414\pm^{0.06}_{0.06}$	0.5 frozen	0.005	$0.9707\pm^{0.008}_{0.008}$	$0.1289\pm^{0.016}_{0.016}$
$LineE$ (keV)	$Sigma$ (keV)	$LineE$ (keV)	$Sigma$ (keV)	N_H (10^{19})	χ^2/ dof		
$6.527\pm^{0.040}_{0.040}$	$0.4838\pm^{0.050}_{0.050}$	$6.445\pm^{0.018}_{0.018}$	0.005	$1.991\pm^{2.432}_{2.408}$	1121.0/870		

Table 7: Her-X1 best-fit parameters. The 0.5 keV Gaussian and the sigma of one iron line have been frozen.

4.4 XTE J1650-500

XMM-Newton observed XTE J1650-500 ($\alpha_{2000} = 16^h50^m1^s.00$, $\delta_{2000} = -49°57'45'.00$) , a X-ray binary as a TOO. The observation used in this report took place on September 13, 2001, revolution 323, lasting more than 23000 seconds.

Spectra have been extracted using single events only neglecting the events at CCD borders and events lower than 0.5 keV:

```
((PATTERN ==1 && FLAG==0 && PI .GE. 500))
```

The spectra have been fit with a model constituted by absorption (wabs), a power law and a blackbody. Several residual features are known to be due to current uncertainties in the calibration.

Fig. 47 shows a plot of XTE J1650-500 (data and model) of the best fit to the PN Burst mode spectrum.

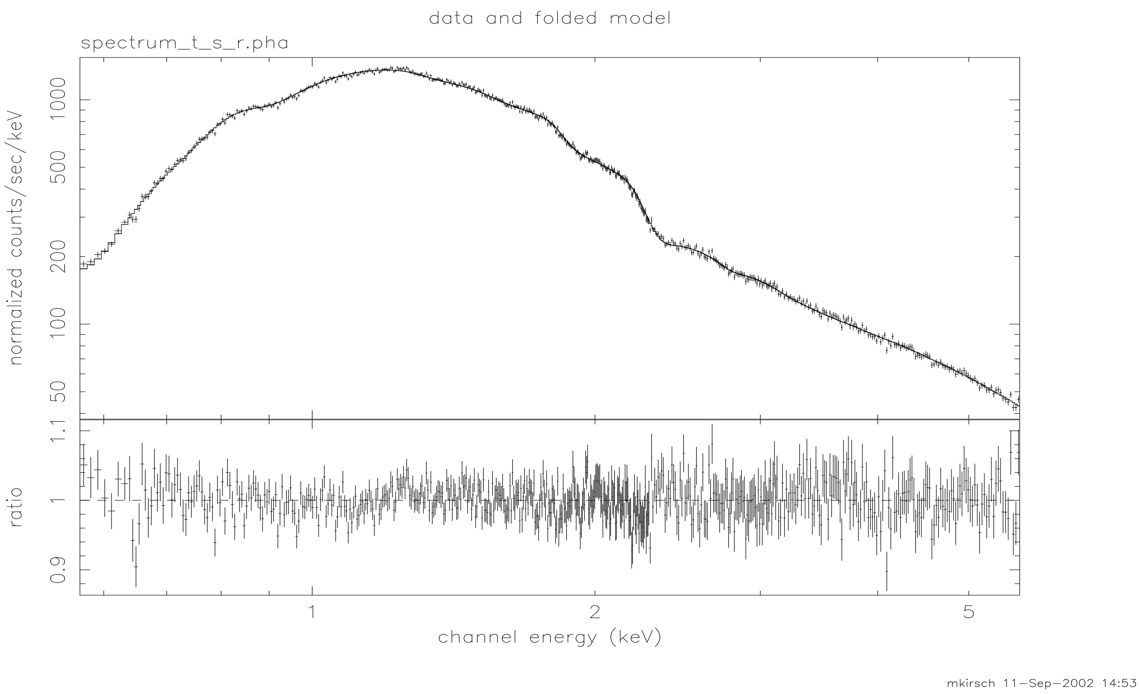

Figure 47: spectrum of XTE J1650 500 in EPIC PN Burst Mode

The best-fit parameters and results are summarized in Tab. 8.

Instrument	Γ	kT_{BB} (eV)	N_{BB}	N_H (10^{22})	χ^2/ dof (keV)
p-n	$3.756\pm^{0.028}_{0.028}$	$1384\pm^{35}_{32}$	$0.091\pm^{0.002}_{0.002}$	$0.7197\pm^{0.0057}_{0.0059}$	648.0/545

Table 8: XTE J1560-500 best-fit parameters.

4.5 RGS effective area

Large changes have been introduced with respect to the RGS effective area not only in the response matrix derivation software in SAS 5.3, but also in several calibration files and corresponding software. They should reduce largely the calibration defects observed previously, reported in earlier validation reports, and discussed largely in Herder (2002). One of the main points was the general agreement between the level of the effective areas of the two RGS instruments while the data showed differences of up to 20%. The effective areas produced by the SAS 5.3 (task *rgsrmfgen*) are given in Fig. 48, showing the expected differences in effective area.

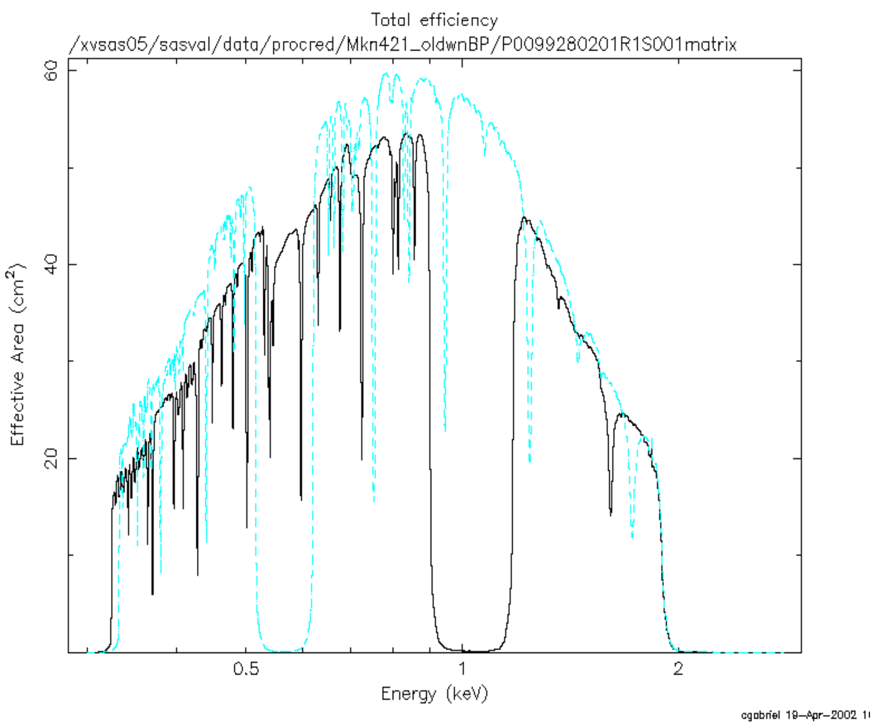

Figure 48: RGS1 (black) and RGS2 (blue) effective areas as derived by SAS 5.3

Using the pipeline reduced data from the Markarian 421 observation, we have fitted simultaneously RGS1 and RGS2 exposures, applying a broken power law model. Up to 1.9 keV the data can be reasonable well fitted, the differences between RGS1 and RGS2 are within less than 10% (previously up to 20 %) as shown in Fig. 49. Also the comparison between first and second order spectra (Fig. 50) shows a good agreement. Fitting first and second order spectra from both RGS together yields the results given in Table 9.

Γ_1	Γ_2	$E_b(keV)$	χ^2/ dof
1.79 ± 0.02	2.57 ± 0.02	0.78 ± 0.1	10045/6833

Table 9: Mkn 421 best-fit parameters fitting a broken power law model to first and second order spectra of RGS1 and RGS2

One of the important instrument features to be calibrated by the new version is the oxygen edge at around 0.55 keV, shown as a defect in former SAS validation reports (see for example the SAS 5.1 validation, Gabriel et al 2001). Fig. 51 shows a zoom image of the O-edge region in the fit of the RGS1 Markarian 421 data.

In addition a simultaneous fit of the RGS and the EPIC PN data (in small window mode)

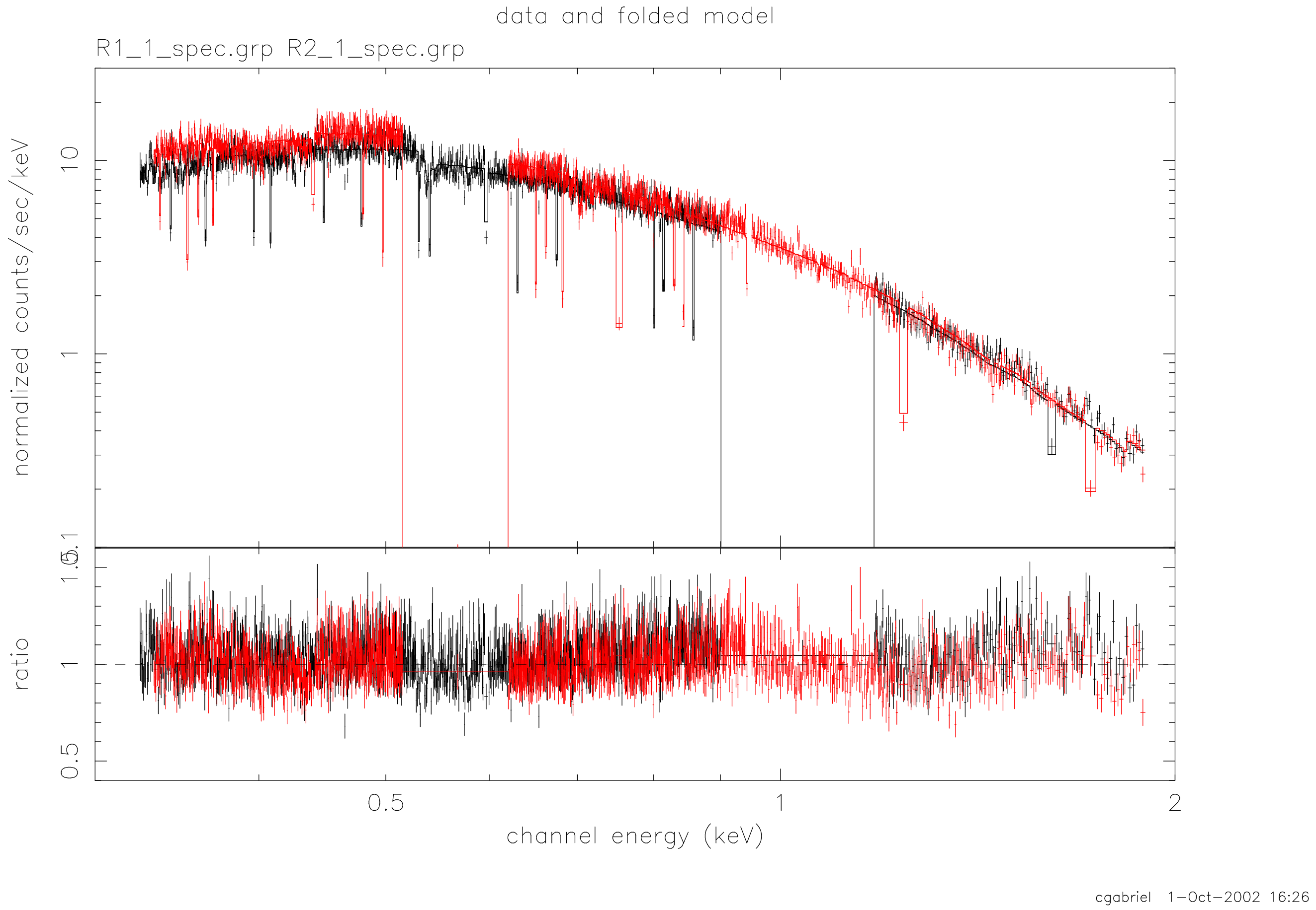

Figure 49: Mkn421 RGS1 (black) and RGS2 (red) spectra fitted with a broken power law model

has been performed in the whole PN range ($E = [0.3 - 12.]$ keV) limiting the RGS data to $E = [0.3 - 1.9]$ keV. The PN data suffers under strong pile-up effects. Before obtaining the PN spectrum, the core of the PSF has therefore been excised. The check against pile-up can be done with the SAS task *epatplot* on the reduced data. Fig. 52 proves that the spectrum extracted is largely free of pile-up effects.

The results (Fig. 53 and table 10) are confirming the large improvements in this version with respect to former ones. There are however still existing discrepancies in the cross calibration (also between the EPIC cameras themselves). The XMM-Newton cross calibration team aims to reduce them to less than 10% in the very near future.

Γ_1	Γ_2	$E_b(keV)$	χ^2/ dof
1.77 ± 0.02	2.55 ± 0.02	0.71 ± 0.1	8366/5717

Table 10: Mkn 421 best-fit parameters fitting a broken power law model to small Window EPIC PN and first order spectra of RGS1 and RGS2 simultaneously

A further simultaneous fit of RGS and EPIC data is shown in Fig. 54. Data corresponding to the observation of PKS 0558-304 in revolution 153, taken with EPIC in windowing modes (see sections 3.1.7 and 4.2.2) and the RGS1 and RGS2 first order data are fitted with a model constituted by a power-law and two blackbodies including galactic absorption. The fit results obtained using only the EPIC data are slightly affected (section 4.2.2). The RGS data do agree within 5% with the EPIC MOS data, except for the low energy region below 0.5 keV and the

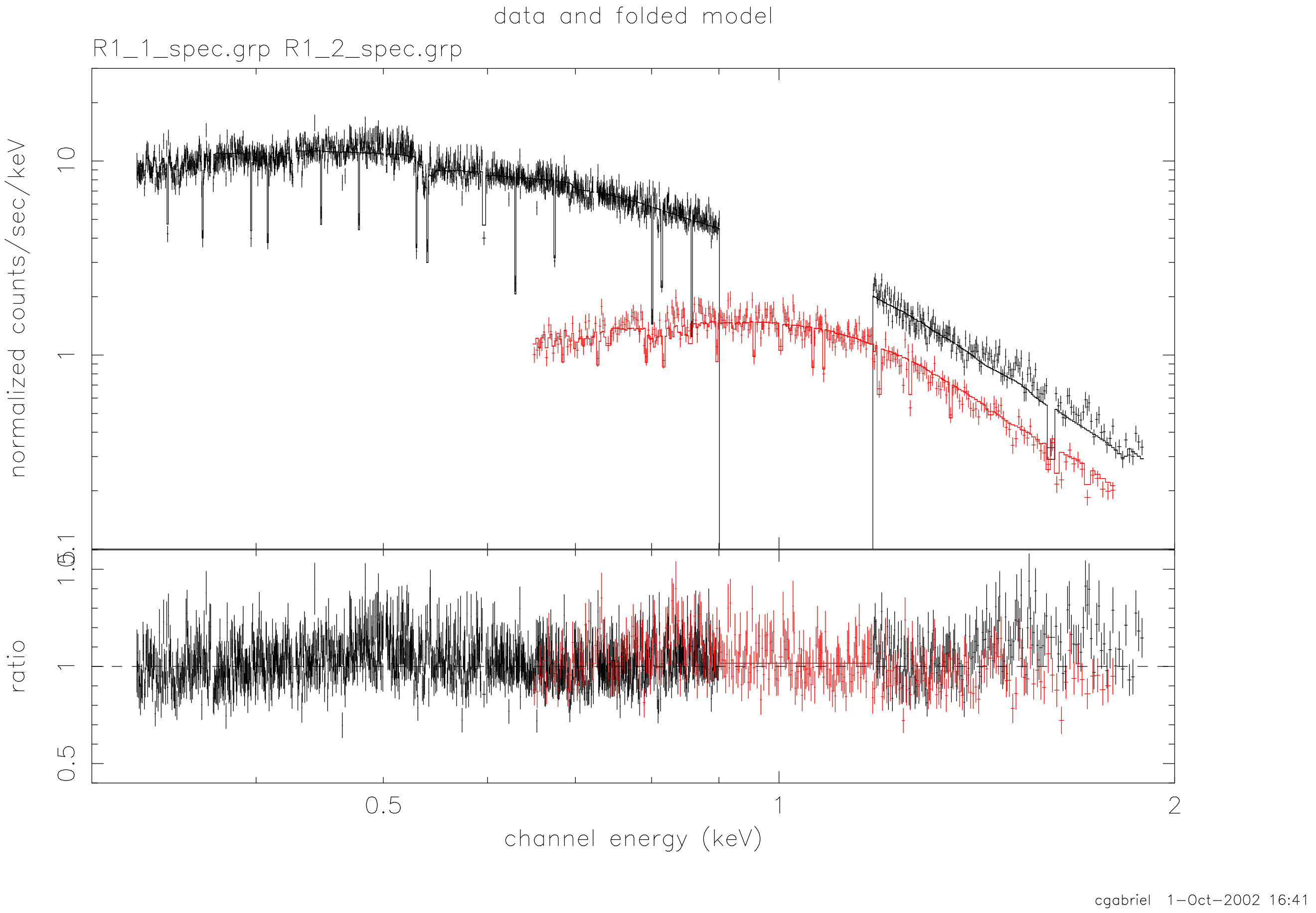

Figure 50: Mkn421 RGS1 first order (black) and second order (red) spectra fitted with a broken powerlaw model

energy range above 1.7 keV, where discrepancies of up to 10-15% are seen.

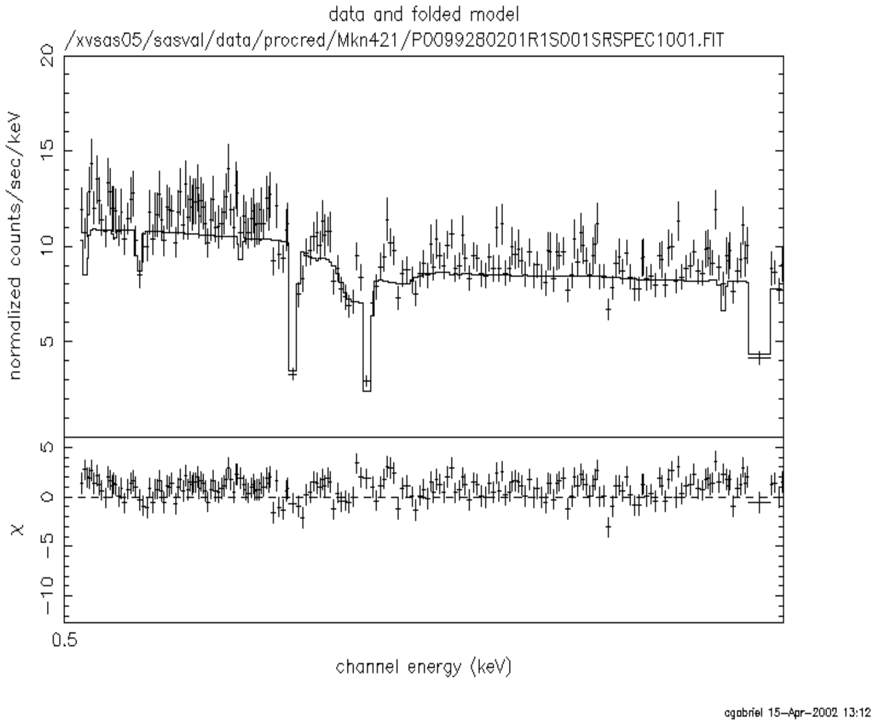

Figure 51: Mkn421 data and fit results of the area around the instrumental oxygen edge (RGS1 first order)

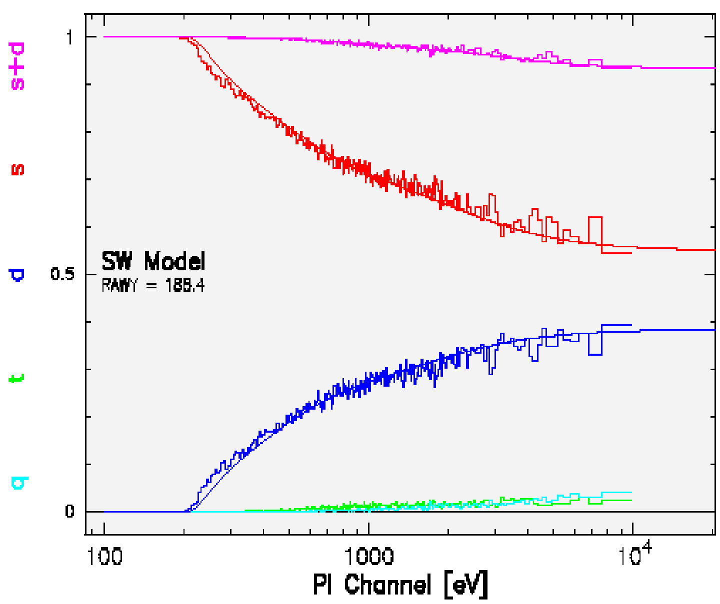

Figure 52: Check of data pattern distributions versus expectations, as produced by the SAS task *epatplot*. Produced after PSF core excision of EPIC-PN data corresponding to the Mkn421 source

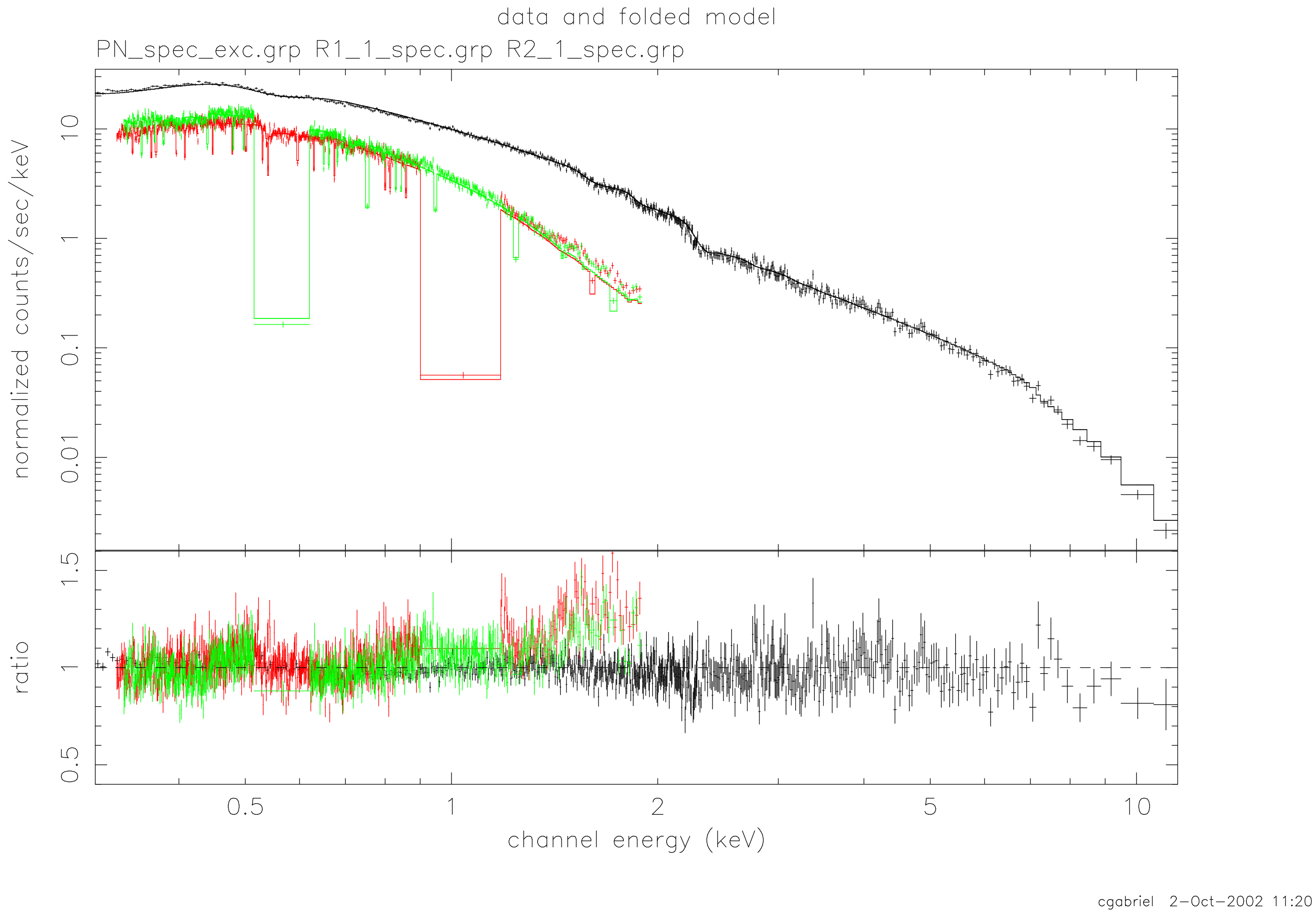

Figure 53: Mkn421 EPIC PN (black), first order RGS1 (red) and RGS2 (green) spectra fitted simultaneously with a broken powerlaw model

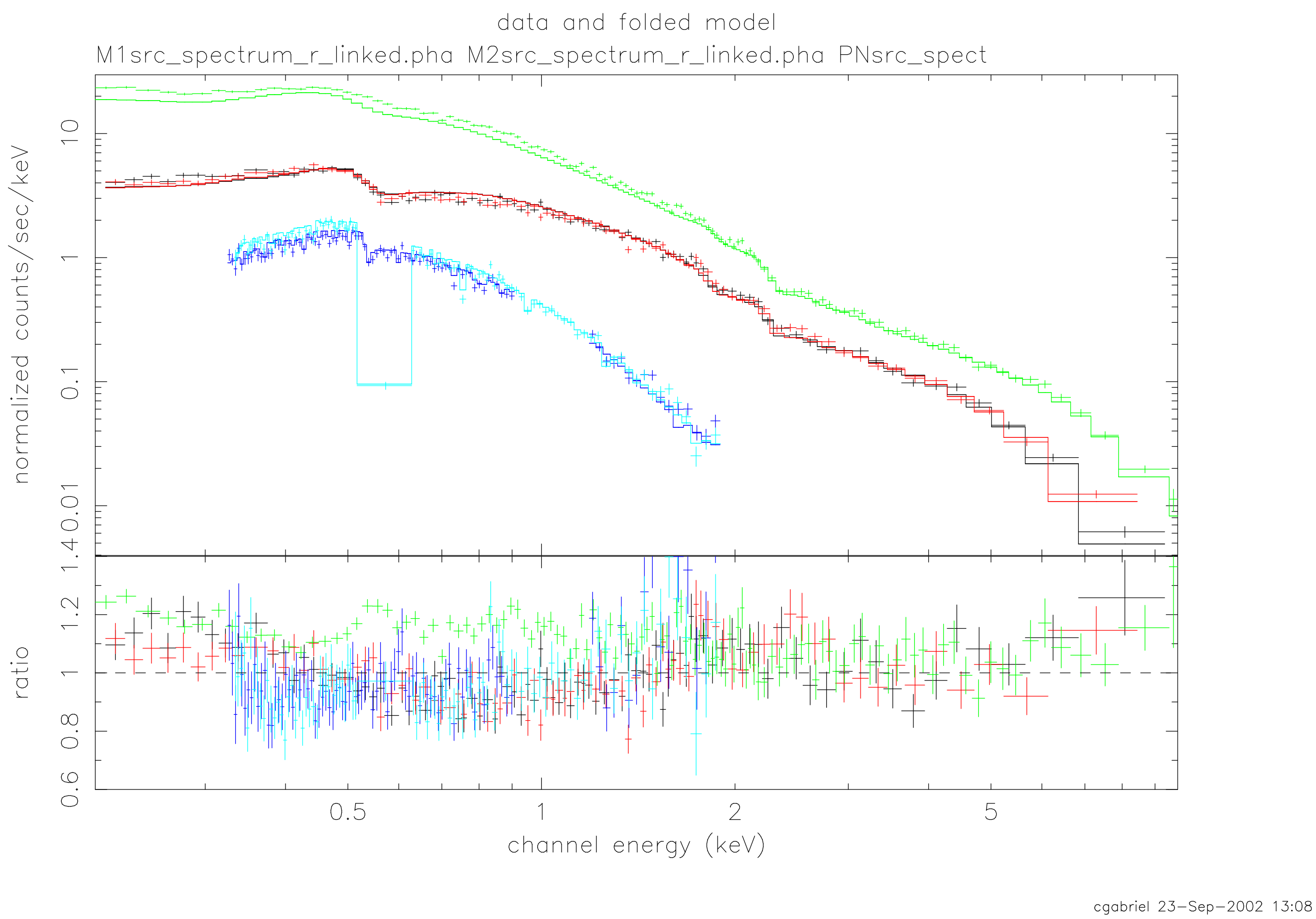

Figure 54: Simultaneous fitting of PKS0558-504 EPIC-PN (green), -MOS1 (black), -MOS2 (red), RGS1 first order (blue) and RGS2 first order (light blue) spectra. Residuals are in units of data/model ratio (*lower panels*).

4.6 RGS wavelength accuracy

In order to assess the wavelength accuracy we have analyzed the data corresponding to the AB Doradus observation in exactly the same way already practiced in the SAS 5.1 validation.

The effective areas produced by the SAS task *rgsrmfgen* within the pipeline are used within XSPEC just for fixing the absolute wavelength scale.

For establishing the wavelength accuracies we have fitted the (raw) data with the sum of a gaussian and a quadratic term in the regions of intense line emission, using a slightly modified version of the IDL function GAUSSFIT (not affecting the results). For the purposes of establishing the position of the main spectral lines this is sufficient in most of the cases, although in some cases due to the non-resolution of multiplets the result is not accurate and visual inspection is made necessary.

Table 11: Spectral lines found in AB Dor - RGS1 and RGS2 - first (first table) and second (second table) order spectrum

		RGS1			RGS2		
Transition	λ_{lab}	λ	**Width**	Δ	λ	**Width**	Δ
Ne X Ly_alpha	12.134 *	—	—	—	12.144	0.024	0.010
Ne IX He_alpha	13.448 P	—	—	—	*13.464*	*0.034*	*0.016*
Fe XVII(27 - 1)	15.014 *	15.022	0.024	0.008	15.026	0.028	0.012
Fe XVIII	16.006 P	*16.030*	*0.043*	*0.024*	*16.007*	*0.013*	*0.001*
Fe XVII(5 - 1)	16.780 *	16.786	0.027	0.006	16.783	0.029	0.003
Fe XVII(3 - 1)	17.055 P	*17.078*	*0.043*	*0.023*	*17.084*	*0.039*	*0.029*
O VIII Ly_alpha	18.969 *	18.977	0.030	0.008	18.981	0.030	0.012
O VII He_alpha (1st)	21.602 *	21.606	0.029	0.004	—	—	—
N VII Ly_alpha	24.781 *	24.783	0.029	0.002	*24.821*	*0.009*	*0.040*
C VI Ly_alpha	33.736 *	33.736	0.030	0.000	33.748	0.041	0.012

The lines in italics are examples of discarded lines by visual inspection. The large widths of the gaussian are due to not resolved multiplets. The Fe XVII(3 - 1) is actually a doublet at 17.053/17.100 A, both components of approximately same intensity. If we take just the reliable lines:
RGS1: $\bar{\Delta} = (4.7 \pm 3.3)$ mÅ $(|\bar{\Delta}| = 4.7$ mÅ)
RGS2: $\bar{\Delta} = (9.8 \pm 3.5)$ mÅ $(|\bar{\Delta}| = (9.8$ mÅ)

		RGS1			RGS2		
Transition	λ_{lab}	λ	**Width**	Δ	λ	**Width**	Δ
Ne X Ly_alpha	12.134 *	12.138	0.016	0.004	12.139	0.021	0.005
Ne IX He_alpha	13.448 P	13.449	0.016	0.001	13.460	0.025	0.012
Fe XVII(27 - 1)	15.014 *	15.014	0.017	0.000	15.017	0.016	0.003
Fe XVIII	16.006 P	16.011	0.016	0.005	*16.007*	*0.013*	*0.001*
Fe XVII(5 - 1)	16.780 *	*16.775*	*0.006*	*-0.005*	16.778	0.021	-0.002
Fe XVII(3 - 1)	17.055 P	*17.076*	*0.037*	*0.021*	*17.076*	*0.036*	*0.021*
O VIII Ly_alpha	18.969 *	18.973	0.018	0.004	—	—	—

Taking the reliable lines:
RGS1: $\bar{\Delta} = (2.8 \pm 2.0)$ mÅ $(|\bar{\Delta}| = 2.8$ mÅ)
RGS2: $\bar{\Delta} = (4.5 \pm 5.0)$ mÅ $(|\bar{\Delta}| = 5.5$ mÅ)

*) RGS-COL-CAL-00-007
P) Phillips et al, A&A Suppl. Ser. 138, 381

Several spectral lines, as found by the procedure, have been compared with literature values. Tables 11 summarize the results for first and second order. No single line was significantly outside the nominal accuracy of 8 mÅ as quoted by the RGS instrument team. However, there is a clear offset towards a positive difference to the literature values, indicating a shift in the whole wavelength scale. The source position used for the whole analysis is derived from the EPIC images. The source is located in the EPIC-PN images close to a CCD gap and in addition suffers under pile-up. The consequence of this is a difference of around 3 arcsec between the derived source centroid and the literature value. Reprocessing of the RGS data using the latter one (as done by the wavelength scale monitoring analysis, see Lorente et al, 2002) proves that the reason for the wavelength scale shift is found in the slightly wrong source position used in the pipeline processing, affecting the whole wavelength scale determination, specially in the case of the RGS2 data. An additional systematic error of around 1-2 mÅ per each arcsec uncertainty in the source position should be expected as a rule of thumb.

In the same framework of the wavelength scale monitoring study it has been shown that the use of the uncorrected spectrum for the wavelength scale determination (as done in this report) does introduce a negligible systematic error (less than 1 mÅ) to the wavelength determination.

4.7 OM interactive results

Using the BPM16274 and Her X-1 data sets several items were checked:

4.7.0.1 Astrometry

Cross correlation of the sources found in the BPM 16274 field with the USNO catalogue (268 common sources) shows a rms difference of [1-2]". It should be noted that PPS does not perform cross correlation with catalogues. This is possible using SAS, if the user provides the input catalogue.

4.7.0.2 Photometry

The optical filters (U,B,V) are correctly treated, including colour corrections for blue and red stars. Errors are less than 5%. A systematic offset in V of about 0.05 mag, has been corrected with the new zero points implemented with the calibration file OM_COLORTRANS_0007 (see release note XMM-CCF-REL-120).

The UV filters (UVW1, UVM2, UVW2) have a bug in the extrapolation of the count rate to the photometry aperture of 35 pix. radius. This underestimates the count rate, specially for bright stars.

4.7.0.3 Source detection

The source detection algorithm is very sensitive to extended background features, as the OM straylight artifacts. This makes that the main source, close to the central straylight patch, very often is not detected. A manual run of the SAS task *omdetect* with non default parameters is adviced to circumvent this problem.

5 Summary

The SAS 5.3.x validation has shown that:

- all instrumental modes currently offered to the XMM-Newton observers are in principle fully supported by the SAS V5.3.3, except for OM grisms observations,
- the specified output products from the default pipeline processing are considered satisfactory and a good basis for full scientific exploitation of the performed observations,
- shortcomings in the calibration do exist in several areas, although a large improvement with respect to the former SAS version (SAS V5.2) has been achieved,
- main object of critical study is the cross calibration among the X-ray instruments,
- the EPIC MOS timing mode has still to be calibrated,
- problems and caveats found by the data analysis are reported along this report, and have been correspondingly noticed in the context of the configuration control of the further SAS development.

Appendix A: calibration files used

The following calibration files have been used by the complete data reduction chain, including PPS and interactive analysis[1]:

```
EMOS1_ADUCONV_0011
EMOS1_BACKGROUND_0001
EMOS1_BADPIX_0009 (G21.5.09, Lockman)
EMOS1_BADPIX_0010 (PKS0558-304 -both)
EMOS1_BADPIX_0011 (AB Dor, Mkn421)
EMOS1_BADPIX_0012 (BPM 16274, Her X-1, XTE J1650)
EMOS1_BADPIX_0015 (PKS2155-304)
EMOS1_CALSOURCEDATA_0001
EMOS1_CTI_0006
EMOS1_DARKFRAME_0007 (all but ...)
EMOS1_DARKFRAME_0009 (PKS2155-304, XTE J1650)
EMOS1_EFFICIENCY_0001
EMOS1_FILTERTRANSX_0009
EMOS1_HKPARMINT_0007
EMOS1_LINCOORD_0016
EMOS1_MODEPARAM_0006
EMOS1_PATTERNLIB_0005
EMOS1_QUANTUMEF_0010
EMOS1_REDIST_0012
EMOS1_TIMECORR_0003
EMOS2_ADUCONV_0011
EMOS2_BACKGROUND_0001
EMOS2_BADPIX_0009 (G21.5.09, Lockman)
EMOS2_BADPIX_0010 (PKS0558-304 -both)
EMOS2_BADPIX_0011 (ABDor, Mkn421)
EMOS2_BADPIX_0012 (BPM 16274, Her X-1, XTE J1650)
EMOS1_BADPIX_0015 (PKS2155-304)
EMOS2_CALSOURCEDATA_0001
EMOS2_CTI_0006
EMOS2_DARKFRAME_0007 (all but ...)
EMOS2_DARKFRAME_0009 (PKS2155-304, XTE J1650)
EMOS2_EFFICIENCY_0001
EMOS2_FILTERTRANSX_0009
EMOS2_HKPARMINT_0007
EMOS2_LINCOORD_0016
EMOS2_MODEPARAM_0006
EMOS2_PATTERNLIB_0005
EMOS2_QUANTUMEF_0010
EMOS2_REDIST_0012
EMOS2_TIMECORR_0003
EPN_ADUCONV_0055 (G21.5.09, Lockman, both PKS0558-504)
EPN_ADUCONV_0077 (Mkn 421)
EPN_ADUCONV_0082 (AB Dor)
EPN_ADUCONV_0093 (BPM 16274, Her X-1)
EPN_ADUCONV_0107 (PKS2155-304, XTE J1650-500)
EPN_BACKGROUND_0001
```

[1] in the cases with no source name related, the file was identified as valid for all datasets

EPN_BADPIX_0054 (G21.5.09, Lockman, both PKS0558-504)
EPN_BADPIX_0069 (Mkn 421)
EPN_BADPIX_0071 (AB Dor)
EPN_BADPIX_0074 (Her X-1)
EPN_BADPIX_0078 (BPM 16274)
EPN_BADPIX_0092 (PKS2155-304, XTE J1650-500)
EPN_CALSOURCEDATA_0001
EPN_CTI_0008
EPN_DARKFRAME_0001
EPN_EFFICIENCY_0001
EPN_FILTERTRANSX_0012
EPN_HKPARMINT_0004
EPN_LINCOORD_0009
EPN_MODEPARAM_0003
EPN_PATTERNLIB_0001
EPN_QUANTUMEF_0010
EPN_REDIST_0007
EPN_TIMECORR_0005
OM_ASTROMET_0008
OM_BADPIX_0004
OM_COLORTRANS_0006
OM_DARKFRAME_0003
OM_DIFFUSEGALA_0001
OM_HKPARMINT_0003
OM_LARGESCALESENS_0002
OM_LINCOORD_0001
OM_PHOTTONAT_0003
OM_PIXTOPIXSENS_0003
OM_PSF1DRB_0004
OM_QUICKMAG_0002
OM_ZODIACAL_0001
RGS1_ADUCONV_0006(G21.5.09, Lockman, both PKS0558-504)
RGS1_ADUCONV_0009(Mkn421)
RGS1_ADUCONV_0010 (AB Dor, BPM 16274, Her X-1, PKS2155-304, XTE J1650-500)
RGS1_BACKGROUND_0001
RGS1_BADPIX_0005 (all but ...)
RGS1_BADPIX_0007 (XTE J1650-500)
RGS1_BADPIX_0008 (PKS2155-304)
RGS1_CALSOURCEDATA_0001
RGS1_CLOCKPATTERNS_0001
RGS1_CROSSPSF_0003
RGS1_CTI_0002
RGS1_DARKFRAME_0004
RGS1_EXAFS_0001
RGS1_HKPARMINT_0009 (G21.5.09, Lockman, both PKS0558-504)
RGS1_HKPARMINT_0010 (Mkn421)
RGS1_HKPARMINT_0011 (AB Dor, BPM 16274, Her X-1, PKS2155-304, XTE J1650-500)
RGS1_LINCOORD_0008
RGS1_LINESPREADFUNC_0004
RGS1_MODEPARAM_0005
RGS1_QUANTUMEF_0007
RGS1_REDIST_0004

RGS2_ADUCONV_0007 (G21.5.09, Lockman, both PKS0558-504)
RGS2_ADUCONV_0010 (Mkn 421)
RGS2_ADUCONV_0011 (AB Dor)
RGS2_ADUCONV_0012 (BPM 16274, Her X-1, PKS2155-304, XTE J1650-500)
RGS2_BACKGROUND_0001
RGS2_BADPIX_0005 (all but ...)
RGS2_BADPIX_0007 (XTE J1650-500)
RGS2_BADPIX_0008 (PKS2155-304)
RGS2_CALSOURCEDATA_0001
RGS2_CLOCKPATTERNS_0001
RGS2_CROSSPSF_0003
RGS2_CTI_0002
RGS2_DARKFRAME_0004
RGS2_EXAFS_0001
RGS2_HKPARMINT_0008 (G21.5.09, Lockman, Mkn 421, both PKS0558-504)
RGS2_HKPARMINT_0009 (BPM 16274, PKS2155-304, XTE J1650-500)
RGS2_HKPARMINT_0010 (AB Dor, Her X-1)
RGS2_LINCOORD_0008
RGS2_LINESPREADFUNC_0004
RGS2_MODEPARAM_0005
RGS2_QUANTUMEF_0008
RGS2_REDIST_0004
XMM_ABSCOEFS_0004
XMM_BORESIGHT_0016
XMM_MISCDATA_0014
XRT1_XAREAEF_0008
XRT1_XENCIREN_0003
XRT1_XPSF_0005
XRT2_XAREAEF_0009
XRT2_XENCIREN_0003
XRT2_XPSF_0005
XRT3_XAREAEF_0008
XRT3_XENCIREN_0003
XRT3_XPSF_0003

Appendix B: observing modes nomenclature

SAS 5.3.x uses the internal modes nomenclature (eg. by the *odfbrowser* output). Find as a help in the following the correspondence between this nomenclature and the one used for the proposer info:

Table 12: Correspondence between external and internal modes denomination

Instrument	**Mode - external name**	**Mode - internal name**
EPIC MOS	Full Frame	Prime Full Window
	Small Window	PrimePartialW2
	Large Window	PrimePartialW3
	Timing	FastUncompressed
EPIC PN	Full Frame	PrimeFullWindow
	Large Window	PrimeLargeWindow
	Small Window	PrimeSmallWindow
	Timing	FastTiming
	Burst	FastBurst
	Extended Full Frame	PrimeFullWindowExtended
RGS	Spectroscopy HCR	HighEventRateWithSES (*)
	Spectroscopy	HighEventRateWithSES (*)
OM	Imaging	Image
	Fast mode	Fast

(*) Both RGS spectroscopy modes are basically the same. The only difference is that HCR does not contain interleaved diagnostic exposures

Acknowledgment

The authors acknowledge a careful reading and useful comments from J.W.den Herder and R.Saxton.

References

XMM-Newton SAS scientific validation Plan, C. Gabriel et al, XMM-SOC-SW-VVP-0016, V1.0, January 2002

Warwick R.S, et al, 2001, A&A, 365, L248

The ROSAT Deep Survey, VI. X-ray sources and optical identifications of the Ultra Deep Survey, Lehman I., Hasinger G., Schmidt M., 2001, A&A, astro-ph/0103368

Absolute astrometry of XMM-Newton fields: eposcorr results, SSC-LUX-TN-0060, Issue 1.0, 13 Nov 2001, Leicester University, Tedds J. & Watson M.

RGS Status of calibration and data analysis, J.W. den Herder & the RGS consortium, XMM-SOC-CAL-TN-0024, V1.0, January 2002

XMM-Newton SAS scientific validation - SAS V5.1, C. Gabriel et al, XMM-SOC-USR-TN-0004, V1.0, August 2001

RGS wavelength scale monitoring results, R. Lorente, A. Pollock, C. Gabriel, 2002, XMM-SOC-CAL-TN-0031, under preparation

O'Brien P.T., Reeves J.N., Turner M.J.L. et al. 2001, A&A 365, L122